

THESIS FOR THE DEGREE OF DOCTOR OF PHILOSOPHY
IN
THERMO AND FLUID DYNAMICS

Aerothermal Study of Intermediate Turbine Ducts

by

MARTIN JOHANSSON

Department of Applied Mechanics
CHALMERS UNIVERSITY OF TECHNOLOGY

Gothenburg, Sweden 2016

Aerothermal Study of Intermediate Turbine Ducts

MARTIN JOHANSSON

ISBN 978-91-7597-308-1

© MARTIN JOHANSSON, 2016

Doktorsavhandlingar vid Chalmers tekniska högskola

Ny serie nr. 3989

ISSN 0346-718X

Department of Applied Mechanics

Chalmers University of Technology

SE-412 96 Gothenburg

Sweden

Telephone: +46 (0)31-772 1000

This document was typeset using L^AT_EX

Printed at Chalmers Reproservice

Gothenburg, Sweden 2016

Aerothermal Study of Intermediate Turbine Ducts

MARTIN JOHANSSON

Department of Applied Mechanics
Chalmers University of Technology

ABSTRACT

An intermediate turbine duct guides the flow from the smaller diameter high pressure turbine to the downstream larger diameter intermediate or low pressure turbine. It is typically equipped with a structural vane transferring loads for the core to the external parts, and supplies the core with necessary services such as oil and air.

Flow in an intermediate turbine duct is highly complex, influenced by the upstream turbine stage flow structures, which include tip leakage flows and non-uniformities originating from the upstream high pressure turbine vane and rotor. The complexity of the flow structures makes predicting them using numerical methods difficult, hence there exists a need for experimental validation.

This thesis includes results from experiments conducted in two different facilities, the Chalmers Large-Scale Low-Speed Turbine Facility and the Oxford Turbine Research Facility. At Chalmers, the emphasis was at aerodynamic measurements including static pressure, total pressure, velocities and flow angles in the intermediate turbine duct. In Oxford, the experimental campaign included both aerodynamic and heat transfer measurements with the purpose of describing the aerothermal flow through the intermediate turbine duct. A new intermediate turbine duct with a medium turning vane was designed, manufactured, instrumented and installed in the Oxford Turbine Research Facility. Three high pressure turbine stage inlet conditions were studied; a uniform inlet flow and two low-NO_x swirl profiles. Three adjacent intermediate turbine duct vanes were instrumented in an identical manner, to study the vane-to-vane clocking effect. Instrumentation includes static pressure tappings and thin film heat flux gauges installed on the intermediate turbine duct vane and endwalls at discrete locations. A three-hole pressure probe equipped with thermocouples above and below was traversed at intermediate turbine duct exit. Steady and unsteady CFD predictions were performed of the intermediate turbine duct on its own and the full 1.5 high pressure turbine stage.

The results from the test campaign in Oxford show the clocking effect to have a larger effect on the surface aerodynamics and heat transfer of the intermediate turbine duct vane than the introduction of a low-NO_x swirl profile at the high pressure turbine stage inlet. The clocking effect is for example seen to change the incidence to the intermediate turbine duct vane. The change in inlet condition is seen to have local effects in the intermediate turbine duct. The CFD results are found to in general match the experimental data fairly well, both in aerodynamics and heat transfer. A comparison of steady and averaged time averaged unsteady CFD is noted to provide similar results.

Keywords: Experimental, Aerodynamics, Heat Transfer, Gas Turbine, Intermediate Turbine Duct

*Darkness cannot drive out darkness: only light can do that.
Hate cannot drive out hate: only love can do that.
- Martin Luther King Jr.*

LIST OF PUBLICATIONS

This thesis is based on the work contained in the following publications:

- 1 M. Johansson, V. Chernoray, L. Ström, J. Larsson and H. Abrahamsson, 2011, Experimental and Numerical Investigation of the Aerodynamics of an Intermediate Turbine Duct, *Proceedings of ASME Turbo Expo 2011*, GT2011-46221, June 6-10, Vancouver, Canada
- 2 M. Johansson, K. Chana, T. Povey, F. Wallin and H. Abrahamsson, 2014, Aerodynamic and Heat Transfer Measurements on an Intermediate Turbine Duct Vane, *Proceedings of ASME Turbo Expo 2014*, GT2014-26032, June 16-20, Düsseldorf, Germany
- 3 M. Johansson, K. Chana, T. Povey, J. Mårtensson and H. Abrahamsson, 2015, Aerothermal Measurements and Predictions of an Intermediate Turbine Duct Turning Vane, *Proceedings of ASME Turbo Expo 2015*, GT2015-43449, June 15-19, Montreal, Canada
- 4 M. Johansson, K. Chana, T. Povey and H. Abrahamsson, 2015, Effect of Low-NOx Combustor Swirl Clocking on ITD Vane Aerodynamics with an Upstream HPT Stage - an Experimental and Computational Study, *Submitted for publication in a scientific journal*
- 5 M. Johansson, K. Chana, T. Povey and H. Abrahamsson, 2015, Effect of Low-NOx Combustor Swirl Clocking on ITD Vane Heat Transfer with an Upstream HPT Stage - an Experimental and Computational Study, *Submitted for publication in a scientific journal*

ACKNOWLEDGEMENTS

Firstly I would like to thank my supervisors, Valery Chernoray and Hans Abrahamsson, for offering me the opportunity to be a part of this project. They have taught me a lot during these years and it has been a pleasure. Hans has especially been a great support throughout the project, always making sure we are moving in the right direction. I would also like to thank Thomas Povey and Kam Chana, who kindly welcomed me to University of Oxford, and guided me through my work with the OTRF. The help with manufacturing instrumentation and running the OTRF from David Cardwell, Sunny Chana, Trevor Godfrey, David O'Dell, and Pete Fair is also to be mentioned – it was greatly appreciated. Thanks also to Fredrik Wallin for fruitful discussions and help with CFD along the way and to Jonathan Mårtensson for his help with CFD work.

Great thanks to all present and past colleagues and friends at Chalmers and in Oxford, for creating an excellent work environment with engaging discussions and plenty of laughter, both at and outside of work.

Last, I would like to thank my family, who always supports me no matter what, as well as my fiancée Hanna who has been an immense support and inspiration throughout this PhD and I am so grateful for it.

This work is funded by the National Aviation Engineering Research Programme (NFFP), lead by the Swedish Armed Forces, the Swedish Defence Materiel Administration and the Swedish Governmental Agency for Innovation Systems. The first part of this work has been carried out at the Department of Applied Mechanics, Division of Fluid Dynamics at Chalmers University of Technology, in co-operation with GKN Aerospace. The second part has been carried out at University of Oxford, in co-operation with GKN Aerospace and Rolls-Royce PLC within Full Aerothermal Combustor Turbine interactiOn Research (FACTOR). The research leading to those results has received funding from the European Union Seventh Framework Programme (FP 7/2007 - 2013) under grant Agreement n° 265985 (www.factor-fp7.eu/).

NOMENCLATURE

Glossary

C_{ITDV}	ITD vane true chord.
C_M	Mach number coefficient.
C_β	Yaw angle coefficient.
C_{p0}	Total pressure coefficient.
I	Electrical current [A].
I_{in}	Constant electrical current through gauge [A].
N	Number of points in sampled signal.
R	Electrical resistance [Ω].
R_{in}	Electrical resistance at T_{in} [Ω].
T	Temperature [K].
T'_w	Corrected wall temperature [K].
T_g	Gas temperature [K].
T_w	Wall temperature [K].
T_{01}	Total temperature [K].
T_{03}	Total temperature [K].
T_{aw}	Adiabatic Wall Temperature [K].
T_{in}	Temperature when $R = R_{in}$ [K].
V	Voltage [V].
V_{in}	Initial voltage [V].
α	Diffusivity [m^2/s].
$\alpha_{R/T}$	Temperature coefficient of resistivity [1/K].
\dot{m}	Mass flow rate [kg/s].
γ	Ratio of specific heat.
M	Mach number.
Nu	Nusselt number.
Pr	Prandtl number.
Re	Reynolds number.
\overline{T}_{01}	Time averaged total temperature [K].
c_1	Coefficient.
c_2	Coefficient.
c_3	Coefficient.
h	Heat transfer coefficient.
h_{Imp}	Impulse response function.
i	Summation variable.
k	Thermal conductivity [W/mK].
n	Sample number.
p_{01}	Total pressure [Pa].
p_{03}	Total pressure [Pa].
p_{avg}	Pressure, averaged [Pa].
p_a	Pressure, left probe tube [Pa].

p_b	Pressure, middle probe tube [Pa].
p_c	Pressure, right probe tube [Pa].
q	Heat flux [W/m^2].

Acronyms

BPR	Bypass Ratio.
CFD	Computational Fluid Dynamics.
FACTOR	Full Aerothermal Combustor Turbine interaction Research.
HPT	High Pressure Turbine.
IPT	Intermediate Pressure Turbine.
ITD	Intermediate Turbine Duct.
LPT	Low Pressure Turbine.
LSLS	Large-Scale Low-Speed.
LVDT	Linear Variable Differential Transformer.
NFFP	National Aviation Engineering Research Programme.
NGV	Nozzle Guide Vane.
OTRF	Oxford Turbine Research Facility.
TFHFG	Thin-Film Heat Flux Gauge.

CONTENTS

Abstract	i
List of publications	v
Acknowledgements	vii
Nomenclature	ix
Contents	xi
I Extended Summary	1
1 Introduction	1
1.1 Description of work	3
1.2 Aims	3
2 Background	5
3 Experimental facilities	9
3.1 Different turbine facilities	9
3.2 Chalmers LSLS Turbine Facility	9
3.2.1 The NFFP5 ITD design	10
3.3 Oxford Turbine Research Facility	11
3.3.1 The FACTOR ITD design	12
3.3.2 Swirl generator	14
4 Instrumentation	17
4.1 Chalmers LSLS Turbine Facility	17
4.2 Oxford Turbine Research Facility	17
4.2.1 Static pressure tapings	19
4.2.2 Thin film heat flux gauges	20
4.2.3 Probe	27
4.2.4 Other Instrumentation	29
4.2.5 Acquisition System	29
4.2.6 Uncertainty	30
5 CFD methodology	33
6 Lessons Learned	37
7 Summary of papers	39
7.1 Paper A	39
7.1.1 Summary	39

7.1.2	Comments	39
7.2	Paper B	40
7.2.1	Summary	40
7.2.2	Comments	40
7.3	Paper C	41
7.3.1	Summary	41
7.3.2	Comments	41
7.4	Paper D	42
7.4.1	Summary	42
7.4.2	Comments	42
7.5	Paper E	43
7.5.1	Summary	43
7.5.2	Comments	43
8	Concluding remarks	45
	Bibliography	47
A	Additional Results	51
B	Pictures of the experimental facility	55
II	Appended Papers A–E	65

Part I

Extended Summary

This thesis focuses on the aerothermal flow through an intermediate turbine duct, mainly conducted through experiments. It consists of an extended summary and five appended papers. Below, an introduction is given and the aims of the research are established. Chapter 2 gives a background to the field describing the complexity of the flow in an intermediate turbine duct and previous research carried out. The experimental facilities and the configurations used in this study are described in Chapter 3 along with a discussion around the use of different facilities. Chapter 4 describes the instrumentation used in the measurements, their design, manufacture, calibration, and associated uncertainty. The set-ups of the Computational Fluid Dynamics (CFD) models from which results are included in the appended papers are depicted in Chapter 5. What in retrospect could have been done differently to further improve the results is discussed in Chapter 6, where suggestions of what can be utilized in coming projects are included. Chapter 7 summarizes the appended papers and Chapter 8 presents conclusions drawn from the results of this thesis. Two appendices are included with additional results not included in the appended papers and pictures of the experimental facilities. Part II of this thesis includes the appended papers.

1 Introduction

In an aero engine the Intermediate Turbine Duct (ITD) is situated between the upstream High Pressure Turbine (HPT) and downstream Intermediate Pressure Turbine (IPT) or Low Pressure Turbine (LPT), depending on engine configuration. It serves the purpose of guiding the flow from a relatively small diameter HPT to a larger diameter IPT or LPT. Typically it includes a vane, transferring structural loads from the core of the engine to external parts, as well as supplying oil and air to the core. An axial cross-section of a typical ITD is shown in Figure 1.0.1 together with its neighbouring components. In today's engine development there is a trend towards higher Bypass Ratios (BPRs). This demands a larger diameter fan, which in turn decreases the rotational speed due to limitations in fan tip velocity. To power the larger fan, a larger LPT is needed, achieved either by increasing the number of stages and/or increasing its diameter. Moving towards the latter choice has the benefit of for example saving overall weight. However, an increase in LPT diameter requires an ITD with a larger radial offset. This can be dealt with by either extending the axial length of the ITD and hence adding weight, or by designing it to be more aggressive, i.e. increasing its radial offset while keeping its axial length. To keep the engine cost and weight down the latter alternative is the preferred, although introducing a number of issues that needs addressing in the design process. To keep the performance of the ITD, no flow separation is allowed within it at design conditions. However, by designing it to be more aggressive there is an increased risk of this occurring, especially along the casing close to the inlet and along the hub close to the exit of the

ITD due to adverse pressure gradients, as discussed in Göttlich et al. [1].

The vane within the ITD has historically, when included, only been carrying structural loads and supplying the engine core with services such as oil and air. In today's trend towards higher BPR engines and more aggressive ITDs, there is a scope within letting the vane carry aerodynamic loads, i.e. turning the flow within the ITD. If the duct and vane is designed to deliver an exit flow in accordance with the design inlet conditions of the downstream IPT/LPT, the Nozzle Guide Vane (NGV) upstream of the turbine can be removed. This would allow for an axially shorter and hence lighter component. By designing a vane that carries aerodynamic load, the risk of flow separation within the duct is reduced as the effective curvature seen by the flow is reduced due to an increase in flow path within the ITD. This however, increases the surface friction in the ITD, which contributes to the total pressure losses. The designs evaluated in this thesis feature a low/medium turning vane, giving that the configurations are targeted towards a counter rotating turbine configuration. Meaning that the shafts, and hence high pressure and intermediate/low pressure turbines/compressors spin in opposite directions. Thus, the amount of turning within the ITD, needed to meet the inlet conditions of the downstream IPT/LPT, is reduced.

Also, in modern aero engines where HPT entry temperatures are continually increasing, it is of greater importance to understand the behaviour of the working gas and its effect on its surroundings. With further elevated temperatures in the downstream ITD, use of highly sophisticated materials and cooling needs to be addressed. This increases the manufacturing costs and affects the overall engine performance, as compressed air needs to be taken from upstream components for cooling purposes.

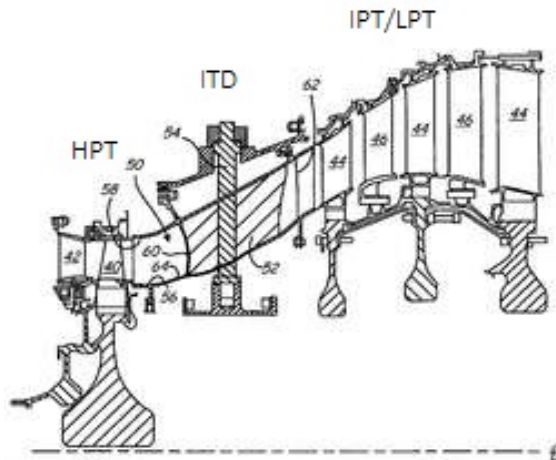


Figure 1.0.1: *Typical ITD in an aero engine, from [2]*

1.1 Description of work

This thesis presents experimental work that was conducted at Chalmers University of Technology and University of Oxford.

The first part describes the work performed at Chalmers, where the Chalmers Large-Scale Low-Speed (LSLS) Turbine Facility has been utilized to investigate the aerodynamics in an ITD equipped with a low turning structural vane. A seven-hole pressure probe was traversed, covering a whole passage both upstream and downstream of the vane and measuring the flow angle, total pressure and velocity fields. The ITD vane was instrumented with static pressure tappings along five spanwise positions. The measurements have been carried out at three different inlet conditions defined as on-design, high load and low load. This was achieved by varying the HPT rotor speed, and hence the HPT rotor exit swirl angle.

The second part describes the work performed at University of Oxford where the Oxford Turbine Research Facility (OTRF), a high-speed transient turbine facility has been utilized to investigate the aerodynamics and heat transfer in an ITD with a medium turning structural vane. This measurement campaign includes an extensive amount of instrumentation throughout the ITD. The aerodynamics was investigated with the use of a three-hole probe traversed downstream of the ITD vane, covering about 1.5 vane passages. Static pressure tappings were included on the ITD vane at three heights as well as on the hub and casing endwalls upstream, in the passage and downstream of the vane. The heat transfer was measured using in-house manufactured Thin-Film Heat Flux Gauges (TFHFGs) that were glued onto the vanes. They are located at three heights and on the casing upstream of the ITD vane. To ensure that the facility is performing in accordance with its design a number of measurements are taken for every run including accelerometers, vibrometers, pressure tappings, thermocouples etc. This thesis includes experimental data taken with three different inlet conditions to the HPT stage: a uniform inlet flow and two low-NO_x swirl profiles (different clocking positions relative to the high pressure turbine vane).

Steady and unsteady CFD was carried out both for comparison with the experimental results and as a tool to further explain the flow through the ITD and its effect on the heat transfer.

1.2 Aims

This research aims to investigate the highly complex flow through an ITD and its influence on the heat transfer of its components. Going in to this project there was an interest in understanding the effect of HPT stage inlet condition on the aerothermal flow through the ITD. The experiments are conducted with the hope to validate current methods used in the industry. During the work, the vane-to-vane clocking effect arose as a topic of interest. There was also some interest in comparing the two experimental facilities to each other to see if the simpler and cheaper continuous facility at Chalmers could provide representative flow phenomena through the ITD.

2 Background

The flow through an ITD is highly complex due to periodical unsteady effects caused by the passing upstream HPT rotor blades. These effects are listed below and interact with each other throughout the ITD.

- Rotor wakes with periodic change in flow angles.
- Secondary flow vortices influencing the boundary layers.
- Rotor tip leakage with high energy flow close to the shroud.
- Substantial swirl angles with spanwise variation.
- Trailing edge shocks in the case of a transonic HPT (not applicable in this study).

The ITD is in essence a diffuser, guiding the flow from a small diameter HPT to a larger diameter IPT/LPT. To understand the flow through an ITD, studies trying to describe individual flow phenomena (as listed above) entering the ITD and its influence on the ITD flow and performance has previously been conducted. At University of Durham a series of experiments were performed to study the influence of blade wakes, swirl, diffusion rates and the inclusion of an ITD vane. Dominy et al. [3] utilised the University of Durham Swan Neck Duct Facility to study an ITD configuration, first with a uniform inlet and then with swirl vanes (axial flat plates) installed looking at the effect of blade wakes on the flow. It was found that the addition of simple blade wakes had a strong influence on the ITD flow in terms of spanwise flow transport within the wake and significant secondary flows that lead to total pressure distortions. It was also shown that a minor distortion at the ITD inlet has disproportionately large influence on the ITD exit flow structure. In Dominy et al. [4] the swirl vanes were turned to generate an ITD inlet flow with a swirl of 15 degrees. The introduction of swirl was shown to skew the rotor wake when passing through the ITD, which in term is shown to change the distribution of loss at the exit compared to the case without inlet swirl. Norris et al. [5] performed experiments looking at the effect of diffusion rates by comparing two different ITD configurations with the same overall area ratio but different axial lengths and hence diffusion rates. It was shown that the spanwise pressure gradient, which strongly influences the secondary flows, was increased around the first bend of the ITD increasing the boundary layer thickness along the shroud and hence the losses within this region. Norris [6] investigated the effect of including a structural vane within the ITD. The shorter duct in Norris et al. [5] was equipped with evenly spaced vanes and a comparison was made. The obvious blockage effect of the vane was noticed to have a severe effect on the total pressure losses within the ITD. However, when including the vane no changes were made to compensate for the reduction in flow area through this part of the ITD. It was also shown to modify the structure of the secondary flows caused by the upstream rotor wakes by suppressing or supporting the boundary layer growth on either side of the vane. When these two flows interact at the trailing edge of the vane, the low energy zone is caused to lift off the shroud surface and create a loss core still visible at the exit of the ITD. The findings by Dominy et al. and Norris et al. were later confirmed in a two part study by Hu et

al. [7] and Zhang et al. [8] who studied the effect of varying the inlet swirl angle either in the top half of the channel or in the bottom. A spanwise migration of fluid within the rotor wake was found and the variation in inlet swirl angles was shown to skew the wake differently through the ITD, affecting the strength of the counter-rotating vortices appearing where the wake meets the endwalls.

While these already mentioned studies describe the effects of individual phenomena they do not address the combination of them, nor do they include any rotating parts, which highly influence the flow through an ITD. Performing studies of this sort demands more complicated test facilities and hence larger funding, especially when introducing rotating parts. The European Union funded two framework 6 projects, AIDA and AITEB-2 that aimed to address this task. A new facility was built at Chalmers University of Technology, used to study both the aerodynamic (AIDA) and the aerothermal (AITEB-2) performance of two different ITD designs downstream of a HPT stage. The facility is of a LSLS type, since many of the flow phenomena found at engine speed can be studied at lower speed. The AIDA configuration was equipped with a vane at the exit of the ITD and measurements included area traverses, static pressure tappings, oil-film visualisation, hot-wire anemometry and LDV, used to in detail describe the flow through this configuration (see Axelsson [9]). Findings included for example the unsteady behaviour of the flow exiting the turbine stage originating from the upstream HPT vane. The AITEB-2 configuration included a structural load carrying vane located further upstream in the ITD. Measurements included area traverses, static pressure tappings, oil-flow visualisation and infra-red thermography (see Arroyo [10]). The focus was on the heat transfer of the ITD and vane, and results showed impacts from the unsteadiness of the upstream stage, as well as wakes from the upstream HPT vane. The impact of the tip leakage flow on the heat transfer of the ITD shroud wall and vane was discussed. As a flight mission includes different operating points where the ITD would experience a variety of inlet conditions, both these configurations were also evaluated under off-design conditions. By altering the turbine speed, the inlet swirl angle was varied. Measurements in the AIDA configuration showed that the off-design conditions changed the flow in the ITD, but the component still managed to deliver an exit flow in accordance with its design, although with a higher pressure loss coefficient (see Axelsson et al. [11]). However, the AITEB-2 configuration (Arroyo et al. [12]), which had its vane located closer to the ITD inlet, showed a significantly larger sensitivity to off-design conditions. The tip-leakage flow was found to impinge, with a high incidence angle, on the suction side of the vane, forming a large vortex. A large separation was found for the low load case (large ITD inlet swirl angle) along the pressure side of the vane close to the hub, due to the difference in swirl angle in the tip-leakage region.

The EU project AIDA also included a rebuild of the Transonic Test Turbine Facility (TTTF) at Graz University of Technology, as described by Göttlich et al. [13], to allow for testing of different ITD configurations. Within AIDA, three different set-ups were studied under various conditions, for example inlet M and HPT rotor tip gap size. These were summarised by Göttlich [14], along with other studies. By increasing the tip gap size, it was found that the total pressure loss was increased. The majority of the total pressure loss in the ITD was generated past the first bend of the ITD, although no difference between the two tip gap sizes was shown here. The difference was instead found further

downstream, where the impact of the tip gap flow is seen in a larger part of the flow field. The third of these configurations was designed to be very aggressive and include flow separation in the ITD, to create a test case to which CFD models can be validated and passive flow control concepts can be tested. It was shown that the efficiency of the separated ITD was very poor, due to a large region of recirculation close to the shroud, around the first bend of the ITD. When comparing with CFD results, it was found that when using mixing planes between the components of the turbine stage, this phenomena was not captured and the pressure losses were under-predicted. In a later EU project (DREAM), a further development of the TTTF included a second rotor, giving a two stage, two shaft turbine facility as described in Hubinka et al. [15]. With this, an integrated concept with splitter vanes installed in between already existing aerodynamic vanes was studied by Spataro et al. [16, 17]. It was found that the integrated concept increased the uniformity of the ITD exit flow, in terms of wakes and secondary vortices, which in turn increased the overall performance of the downstream LPT stage.

Experimental studies of the flow through an ITD has also been performed at the Von Karman Institute of Technology, where the Compression Tube Facility has been utilized. Billiard et al. [18] studied the aero-thermodynamics of an ITD vane, while changing its pitch-wise relative position to the upstream HPT vane between four different positions. The change in relative position altered the inlet conditions to the ITD significantly, due to a change in relative position of the pitchwise variation in total pressure and the potential field coupled to the static pressure of the ITD vane, which affects the ITD inlet M. The main effects on the vane due to clocking were found to be around the leading edge. It was also shown that the thermal load was noticeably reduced for one of the clocking positions. In Lavagnoli et al. [19] and Solano et al. [20], a multi-splitter concept was integrated in the ITD and investigated for three operating conditions. It was equipped with large structural vanes with three smaller aero vanes in between. It was introduced as a way of achieving increased uniformity at the exit of the ITD, as well as integrating the first stator of the downstream turbine stage with the ITD. The structural vane was shown to distort the flow upstream the aero vanes, with larger circumferential non-uniformities. However, the pressure levels at the rear of the vanes is shown to be similar, also for off-design conditions, providing a uniform outlet flow field. When operating the facility at an off-design condition with an ITD inlet flow angle far off the nominal, a large separation appears along the pressure side of the structural vane and the whole vane passage is shown to be affected.

At Ohio State University, the Turbine Test Facility was equipped with a 1.5 stage turbine. Haldeman et al. [21] studied the aerodynamics and heat flux of this configuration, with the facility operating in shock-tube and blowdown modes. The findings showed for example that the normalised pressure data was insensitive to the operation of the facility and the Reynolds number, thus enabling combining aerodynamic data from both operating modes to create a fuller data set. In Haldeman et al. [22] the clocking effect between the upstream HPT vane and the ITD vane was studied by rotating the ITD configuration circumferentially between experiments, to five different positions. Multiple measurement techniques were used, and a notable and consistent change in efficiency for the different clocking positions was reported. The maximum efficiency was obtained when the static pressure was the highest on the ITD vane surface, with the least amount of

variation in both the time and frequency domain. A small effect on the upstream HPT vane was shown to be caused by the ITD vane, and the interaction between the two changed the inlet conditions to the ITD significantly.

Studies of the influence of inlet swirl on the HPT stage has been performed by Qureshi et al. [23]-[24] and Beard et al. [25]. The swirl was found to significantly alter the HPT vane loading near the endwalls, increase the heat transfer on both HPT vane and blade (although less significant on the blade) and a reduction in HPT efficiency mainly due to increased loss generation in the HPT vane passage.

3 Experimental facilities

This chapter gives a brief overview of different experimental set-ups used when studying the flow through aero engine components, discussing advantages and disadvantages. It also describes the facilities used in the investigations presented in this thesis, the Chalmers LSLS Turbine Facility and the OTRF.

3.1 Different turbine facilities

In general, facilities used in aero engine research are divided into rotating and non-rotating, low-speed and high-speed, cold and hot, and continuous and transient facilities. All these variations come with general advantages and disadvantages, and depending on the desired targets and constraints within a project, the most suitable combination of these attributes vary.

A major consideration when designing a new facility is the total cost of building and running it. This is highly affected by what attributes are chosen, for example a rotating facility is in general more complicated to design and more costly to run compared with a non-rotating facility. Rotating facilities offer a more engine realistic flow with complex flow structures, especially when realistic rotational speeds are investigated. However, this introduces issues such as large forces within the facility that needs handling and potentially complex instrumentation paths. Facilities such as the TTTF at Graz University of Technology (Göttlich et al. [13]), the Oxford Rotor Facility at University of Oxford (Ainsworth et al. [26]) and the Chalmers LSLS Turbine Facility (Arroyo et al. [27]) are included in this category. Linear and annular cascades (non-rotational) on the other hand, targets more novel research, where a specific issue is isolated. This could for example include measurements of capacity, vane cooling, or detailed vane aerodynamics and heat transfer (see for example Hjærne et al. [28], Norris [6] and Hu et al. [7]).

When focusing on the heat transfer of an aero engine component, a temperature gradient of some sort is necessary. This could imply either having a hot gas flowing over a cold surface, or a cold gas flowing over a heated surface. In transient high-speed facilities, such as the OTRF at University of Oxford (Chana et al. [29]), the Compression Tube Facility at Von Karman Institute (Paniagua et al. [30]), the Turbine Research Facility at the Air Force Research Laboratory (Anthony et al. [31]) and the Turbine Test Facility at the Ohio State University (Dunn et al. [32]), this is typically solved by introducing a temperature step at the start of a run. This technique is less straightforward to implement in a continuous facility, where either the surface of interest needs to be heated as by Arroyo [10], or a temperature step to be introduced to the test gas when stable conditions are established.

3.2 Chalmers LSLS Turbine Facility

The Chalmers LSLS Turbine Facility is a low-speed large-scale 1.5 stage turbine facility, offering possibilities to study the flow through an ITD. A schematic of the facility is found

in Figure 3.2.1. It was designed within the previous EU programmes AIDA and AITEB-2, where it was utilized for aerodynamic (Axelsson [9]) and heat transfer (Arroyo [10]) measurements in two different ITD configurations, both including a structural vane. The facility was designed to meet the Reynolds number of the corresponding part in a real aero engine, for the results to be associated to what can be expected in a real aero engine. The nominal operating conditions of the facility are found in Table 3.2.1. The facility is powered by a 110 kW centrifugal fan. The test gas (air) is then passing through several flow conditioning devices before reaching the nose cone that splits the flow to annular. The turbine stage, designed within AIDA by Rolls Royce Deutschland (RRD), is designed to be simple, robust and corresponding to the second stage of an unshrouded two-stage HPT, providing a realistic ITD inlet flow. The turbine is kept at constant speed with aid of a hydraulic brake, which converts the mechanical power of the turbine to hydraulic work. The brake load to the turbine is governed by the adjustment of two valves that restricts the oil flow through the hydraulic pump. By this, the facility is tuned to the desired operating point. It can also be used to set off-design conditions by allowing the turbine to spin at a higher or lower speed and hence delivering a different ITD inlet condition, mainly in terms of swirl angle variations.

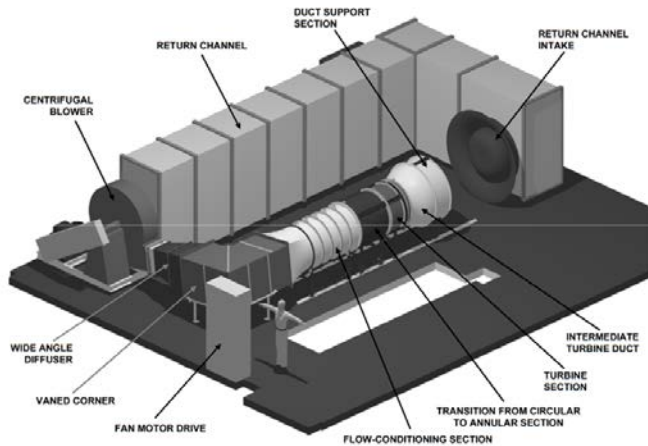


Figure 3.2.1: *Chalmers LSLS Turbine Facility*

3.2.1 The NFFP5 ITD design

The ITD with vane design evaluated in the Chalmers LSLS Turbine Facility was performed at Volvo Aero Corporation (today GKN Aerospace). The same turbine stage used in AIDA and AITEB-2 was reused, setting the inlet conditions to the ITD. It also, to some extent, gave geometric restrictions to the design. The design was targeted to be robust to off-design conditions and engine representative, with low pressure losses and without separations in the ITD. The vane was chosen to be typical for a counter rotating engine system design and hence low turning. The design was performed with the Volvo Aero

Table 3.2.1: Chalmers LSLS Turbine Facility nominal conditions

Parameter	Value
Re based on ITD inlet height	160000
Speed [rpm]	1060
Power [kW]	110
Max turbine pressure ratio	1.06
\dot{m} [kgs ⁻¹]	10

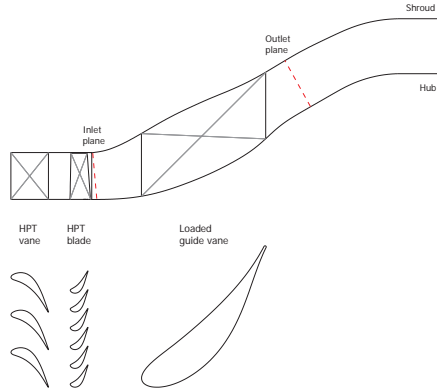


Figure 3.2.2: *Cross-sectional view of the Chalmers Turbine Facility*

in-house tool VolVane and evaluated with ANSYS CFX version 12.1. A meridional view of the HPT stage and the new ITD configuration is presented in Figure 3.2.2 with inlet and outlet evaluation planes, and vane/blade count periodicity included.

3.3 Oxford Turbine Research Facility

The OTRF is a short duration wind tunnel, enabling engine sized turbines to be tested at the correct non-dimensional parameters for aerodynamic and heat transfer measurements (Table 3.3.1). It was initially used as an annular cascade, investigating flows around HPT vanes. Later, a HPT rotor was installed (Hilditch et al. [33]), and the facility was used in several research programmes. In the year 2000 a second vane was introduced and a 1.5 stage HPT was investigated with different HPT stage inlet conditions, see Povey et al. [34] and Chana et al. [35]. A schematic of the facility is shown in Figure 3.3.1 and a cross-section of the working section is included in Figure 3.3.2. The ITD has been isolated

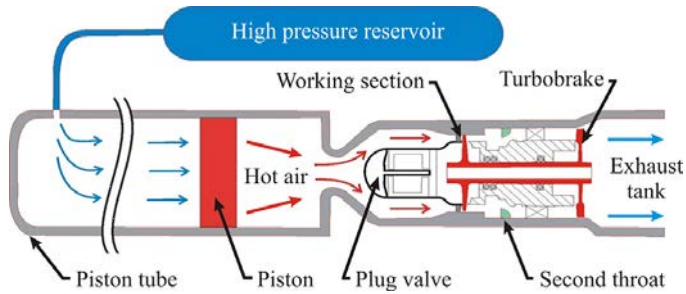


Figure 3.3.1: *Schematic of the OTRF*

from the downstream turbobrake (designed to achieve constant speed) by introducing a choked throat and a novel deswirl vane, of similar type as described by Povey et al. [36]. By correct design of the deswirl vane, the radial static pressure distribution at the ITD exit is maintained. The deswirl vane turns the flow back to axial, to meet the downstream design inlet conditions for the turbobrake. The turbobrake is mounted on the same shaft as the turbine, and matches the turbine power when running at design speed (Goodisman et al. [37]).

In a typical run the HPT rotor is accelerated to design speed, the test gas is isentropically compressed to the desired pressure and temperature by a light piston (driven by a higher pressure upstream), then gas is released into the working section by means of a fast acting plug valve. A typical test results in about 400 ms with steady conditions (see Figure 3.3.3).

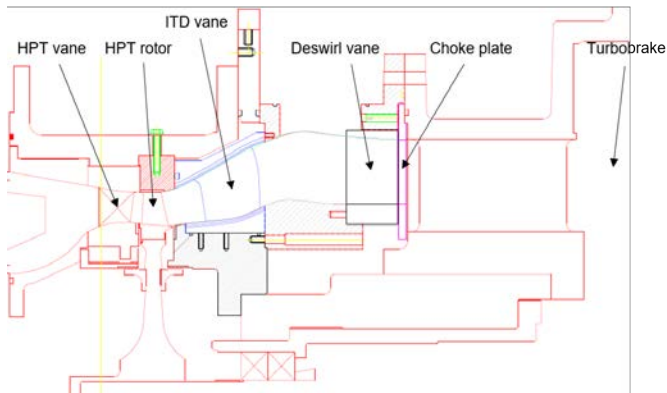


Figure 3.3.2: *Cross-sectional view of the working section*

3.3.1 The FACTOR ITD design

The new ITD configuration was designed using the GKN Aerospace Engine Systems (former Volvo Aero) in-house design tool, VolVane, which contains a 3D Euler solver. To determine the targeted aerodynamic exit condition of the ITD, a throughflow analysis

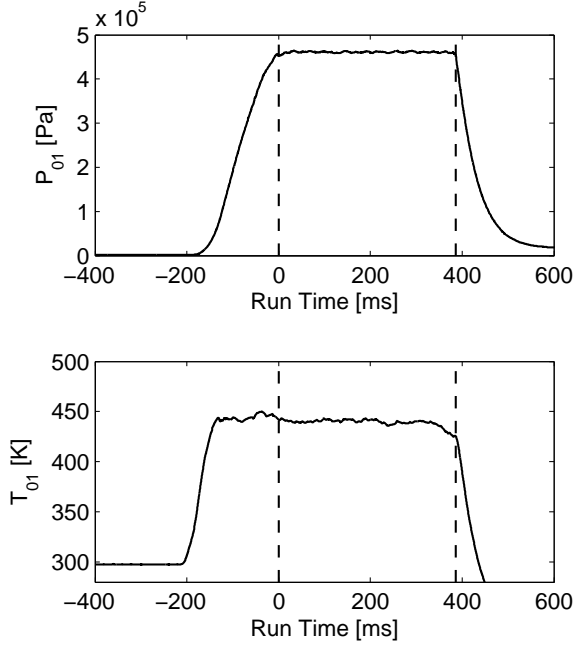


Figure 3.3.3: *HPT vane inlet p_{01} and T_{01} for a typical run*

Table 3.3.1: OTRF nominal conditions

Parameter	Value
Re based on NGV axial chord	1.61×10^6
M at NGV exit	0.879
Speed [rpm]	9500
Mean inlet T_{01} [K]	444
Mean inlet p_{01} (bar)	4.6
Gas to wall temperature T_g/T_w	1.52
\dot{m} [kg s^{-1}]	17.4

was performed at Rolls-Royce Plc using their Q263 code, ahead of designing the ITD with vane. The throughflow analysis provided ITD exit profiles in terms of radial distributions of flow angles, static pressure and Mach number. These, along with geometric constraints, were used as targets in the design process. The geometric constraints were put together so that the final design would be representative for an engine component, although still

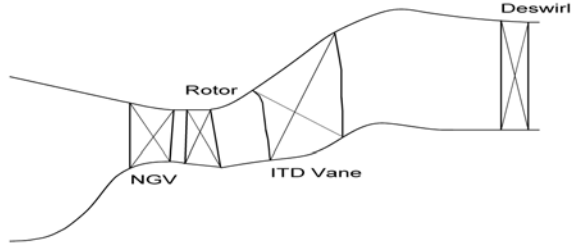


Figure 3.3.4: *Meridional view of the MT1 stage, ITD, and deswirl*

being robust to off-design conditions, without flow separation, shocks and with low total pressure losses. This included measures such as inlet to outlet area ratio, ITD length to inlet height ratio, radial offset to ITD length ratio. There was a desire to keep a few key parts in the facility to reduce the cost of this re-build, which introduced some minor constraints to the final design. The proposed designs (from VolVane) were evaluated using 3D CFD in ANSYS CFX version 12.1, with a fully resolved mesh in the order of 2.2×10^6 number of nodes, the $k - \omega$ SST turbulence model and assuming a fully turbulent flow. Radial profiles based on previously measured and published data from Beard et al. [38], were used as the inlet boundary conditions, to set the flow angles, total temperature and total pressure distributions. A radial static pressure profile was used at the outlet. The design aimed to meet the set ITD exit targets from the throughflow analysis, while also reducing the risk of separation, peak Mach numbers and total pressure loss. A meridional view of the new configuration, including the deswirl vane, and the MT1 HPT stage is found in Figure 5.0.1a. The final design was also evaluated at off-design conditions, to prove its robustness, by varying the radial profile of the ITD inlet swirl angle with ± 10 degrees. The results showed no flow separation in the ITD and the flow was turned to the desired ITD exit swirl angle distribution.

With this new ITD a new deswirl vane design was necessary. Two different designs were evaluated using 3D CFD in ANSYS CFX with different vane counts and chord length. Both performed in accordance with set targets, delivering an axial flow downstream and choking the flow within its passage when introducing a plate at the trailing edge. To increase the axial distance between the ITD vane trailing edge and deswirl vane leading edge, the shorter design with a higher vane count was chosen. This introduces a larger flexibility in accessing the area downstream of the ITD vane to for example traverse a probe.

3.3.2 Swirl generator

To achieve the Swirl 1 and 2 inlet conditions to the HPT vane, a module developed by Qureshi et al. [39] was installed upstream of the stage. The swirl module installed in the OTRF is shown in Figure 3.3.5. It consists of 16 swirlers that turn the flow to a desired profile. The generated swirl profile is representative of extreme exit swirl conditions for a low-NO_x combustor with peak yaw and pitch angles of approximately ± 50 degrees.

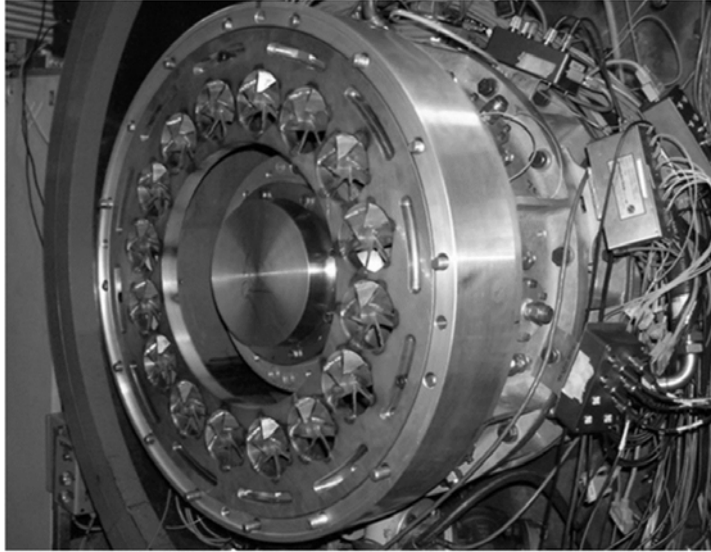


Figure 3.3.5: *Swirl module installed in the OTRF*

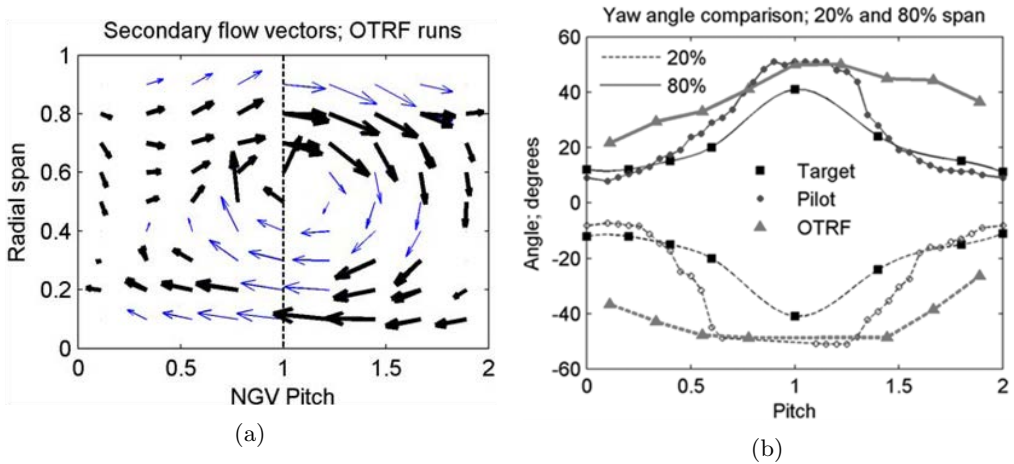


Figure 3.3.6: (a) *Secondary flow vectors profile; measured in OTRF by Qureshi et al. [39].* (b) *Yaw angle profile at 20% and 80% span; comparison of measurements in the OTRF and the pilot study with the target profile by Qureshi et al. [39].*

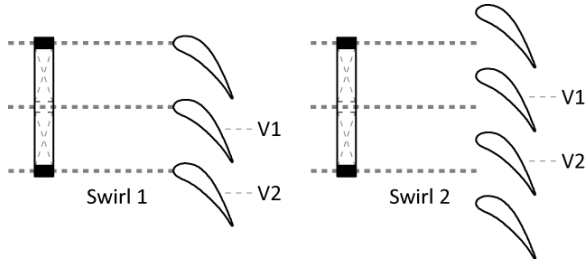


Figure 3.3.7: *Clocking of swirl system relative to HPT vane leading edge*

A vector plot of the secondary flow with results from Qureshi et al. [39] is shown in Figure 3.3.6a. The bold arrows indicate the location of where the measurements were conducted. To aid the visualization, data was interpolated for the internal points and extrapolated for the 10 and 90% points. Figure 3.3.6b show experimental data of the yaw angle distribution at 20 and 80% height taken in a pilot study and when installed in the OTRF compared with the targeted profile. The swirl module was mounted in two positions relative to the HPT vane. The first (Swirl 1) with the core of the swirl profile aligned with the leading edge of every second HPT vane (V1) and the second (Swirl 2) aligned with the passage of every second HPT vane, depicted in Figure 3.3.7.

4 Instrumentation

This chapter includes a description of the instrumentation used in both facilities, and the calibration of said instrumentation.

4.1 Chalmers LSLS Turbine Facility

While running the facility, several measurements are continuously being conducted to monitor the current operating point and surrounding conditions. This includes measures such as turbine speed and torque, hydraulic brake oil temperature, NGV inlet total temperature and pressure, static pressures across the 1.5 stage etc. The measurements are recorded every 2 s and used to determine whether the facility is performing in accordance with its design conditions and when the flow can be considered as steady. The latter is mainly determined by monitoring the change in the hydraulic brake oil temperature, when considered stable so is also the flow.

The aerodynamics data reported in the first appended paper of this thesis were taken with static pressure tappings along the surface of the ITD vane and by traversing a seven-hole pressure probe. The static pressure tappings were located at five heights of the vane (5, 25, 50, 75 and 95%), with denser distribution where larger gradients are expected, such as around the leading edge. The instrumented vane was manufactured with stereolithography (SLA), with the pressure tappings built in. Plastic tubes were attached to each tapping and the recording was carried out with a Scanivalve mechanical multiplexer, connected to a 16-channel PSI 9116 digital pressure scanner with a measuring range of ± 2500 Pa. The mean pressures were evaluated by averaging across 1000 samples acquired at a sampling rate of 500 Hz. The seven-hole probe is of L-type shape, with a 2 mm head and individual distances between the holes of 0.5 mm and a tip half-cone angle of 30 degrees. The calibration of the probe was performed in an open jet flow at a velocity of 25 m/s. The probe is traversed by a three-axis traversing system (cylindrical coordinates), which is powered by three stepper motors, one in each axis direction. The traversing was performed across a two dimensional area covering an ITD vane pitch, i.e. 30 degrees, upstream and downstream of the ITD vane. The location of the measurement planes are indicated as dashed lines in Figure 3.2.2. Measurements were performed with a denser distribution close to the hub and shroud, to better resolve the larger gradients associated with these areas, especially close to the shroud. The data is acquired by the same digital pressure scanner as for the static pressure tapping measurements.

4.2 Oxford Turbine Research Facility

To monitor the performance of the OTRF during a run, a set of standard instrumentation is installed and data is acquired for every run, to determine the quality of the run. This includes measures such as HPT rotor speed, HPT vane inlet total temperature and pressure, HPT vane static pressure distribution at 50% height and endwall static pressures across the 1.5 stage. A tolerance is set for every individual measure, which

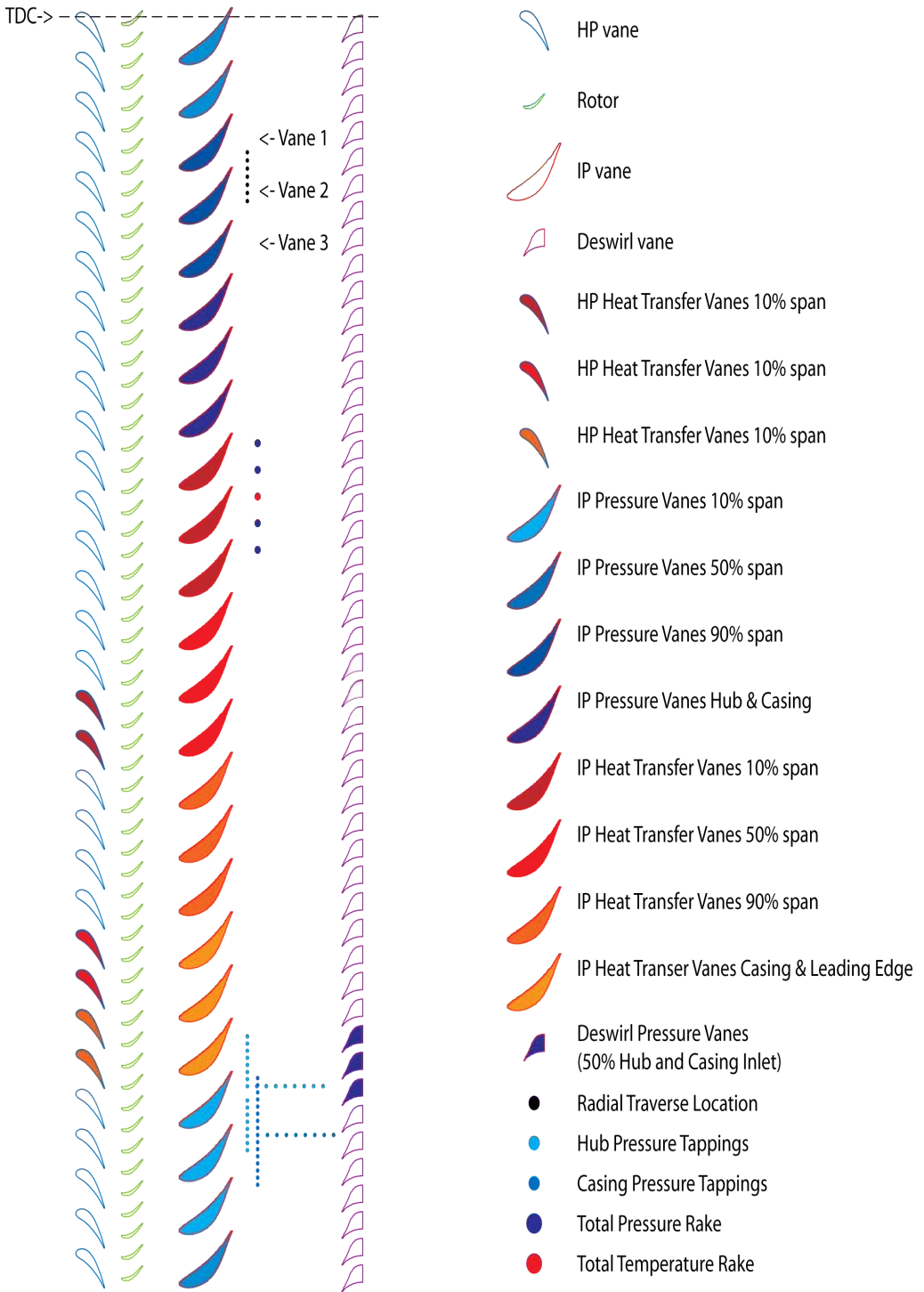


Figure 4.2.1: Instrumentation plan within FACTOR



Figure 4.2.2: *ITD vane instrumented with static pressure tappings at 50% height*

the measurement needs to meet for the run to be considered successful. Most of these measures have been set as standard in multiple research projects over the years in the OTRF, and are considered a standardised way to determine the success of a specific run in the OTRF. A few measures, such as ITD endwall static pressures, are added specifically for this project and their nominal condition are determined during commissioning of the new configuration.

Prior to the design of instrumentation, a preliminary unsteady 1.5 stage CFD prediction was carried out to give guidance into which areas would be of most interest for CFD validation. The results showed an interaction between the HPT vane and the ITD vane due to the difference in vane count between the two (32 HPT vanes and 24 ITD vanes). To investigate this in the experiments, three adjacent vanes were instrumented in an identical manner. A schematic of all the instrumentation installed in the facility for this measurement campaign is presented in Figure 4.2.1.

4.2.1 Static pressure tappings

To measure the static pressure across the surfaces in the ITD, a large number of static pressure tappings were drilled into the endwalls and vane. The tappings have a diameter of 1 mm and a pipe is glued to the outlet of the hole and their connection sealed. A plastic scanivalve tube is then attached to the pipe and taken out of the facility to the pressure transducers. To reduce the length of scanivalve tubing necessary, the pressure transducers were mounted on the OTRF. Figure 4.2.2 shows a typical ITD vane with static pressure tappings at 50% height. In total, twelve vanes are instrumented with tappings, in four different set-ups, giving that three adjacent vanes are instrumented in an identical manner. There are tappings at three heights (10, 50 and 90%) and circumferentially both on hub and shroud; upstream, in the passage and downstream of the ITD vane. The locations of the tappings on the ITDs vane are shown in Figure 4.2.3 and on the ITD endwalls in Figure 4.2.4. There are approximately 20 tappings on each vane and about 40 on each vane pitch platform, giving in total 312 tappings, with a spacing between tappings of

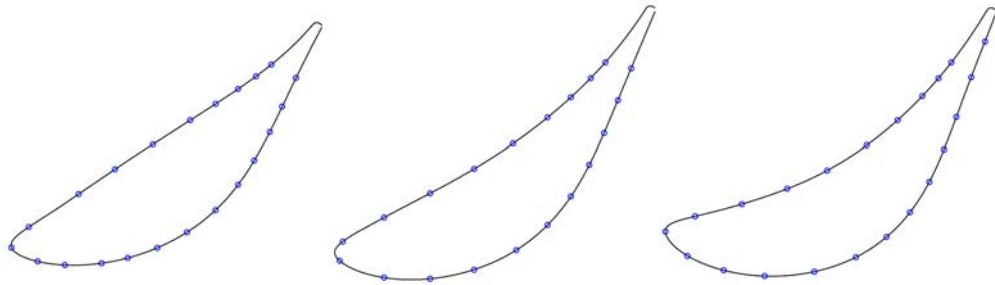


Figure 4.2.3: *Location of static pressure tapings around ITD vane at 10, 50, and 90% height*

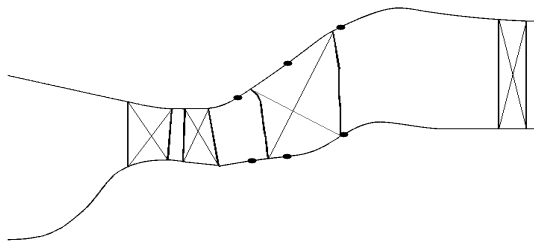


Figure 4.2.4: *Meridional view of the MT1 stage, ITD, and deswirl. The dots show the axial location of the ITD endwall static pressure tapings.*

about 5 mm, measured as surface distance. There are also a number of tapings installed further downstream of the ITD vane, at the exit of the duct, both circumferentially and axially. To make sure the deswirl vane is performing in accordance with what is expected, a deswirl vane has been instrumented with tapings at 50% height as well as upstream of the vane, circumferentially on both hub and shroud.

4.2.2 Thin film heat flux gauges

To measure the heat transfer along the surfaces of the ITD with vane, TFHFGs have been manufactured, annealed, calibrated and installed. This technique has previously been extensively used in the OTRF and has been developed over the years to its current standard, both in terms of manufacturing, data acquisition, and post-processing techniques. Doorly et al. [40] described the theory behind TFHFGs, and Oldfield [41] described the impulse response method used to derive the heat transfer signal from a measurement. The main benefit with this technique is the fast response time, allowing high frequency measurements to investigate the unsteady flow over a surface in a high-speed turbine facility. There are TFHFGs at three heights (10, 50 and 90%) and circumferentially on the casing at two axial locations upstream of the ITD vane. The locations of the TFHFGs on the ITDs vane are shown in Figure 4.2.6 and on the ITD casing in Figure 4.2.7. There



Figure 4.2.5: *ITD vane instrumented with TFHFGs at 90% height*

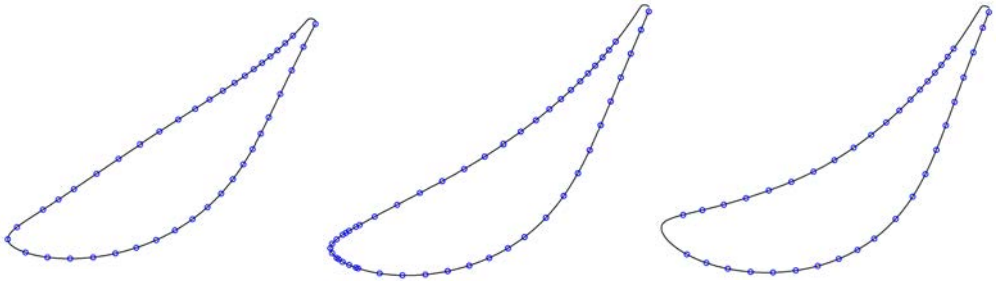


Figure 4.2.6: *Location of TFHFGs around ITD vane at 10, 50, and 90% height*

are approximately 40 gauges on each vane and ten on each vane pitch casing, giving in total 429 gauges.

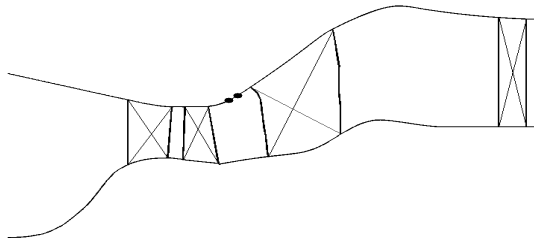


Figure 4.2.7: *Meridional view of the MT1 stage, ITD, and deswirl. The dots show the axial location of the TFHFG on the ITD casing.*

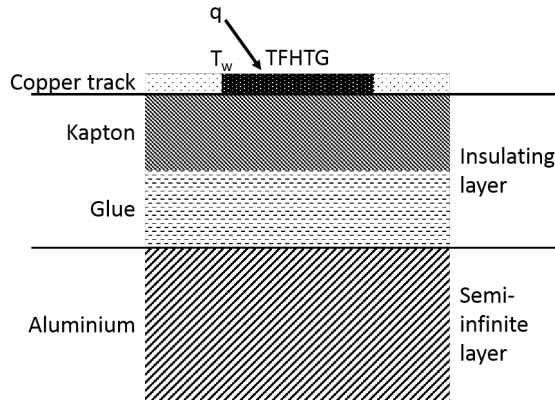


Figure 4.2.8: *Sketch of a TFHFG*

Design

A sketch of a TFHFG is shown in Figure 4.2.8. The design in this campaign consist of the aluminium of the ITD with vane, to which a $50\ \mu\text{m}$ thick sheet of a polyimide (Kapton) with etched out copper tracks is glued, giving the insulating layer a total thickness of $115\ \mu\text{m}$. The thickness of the copper tracks is $18\ \mu\text{m}$. The TFHFG is then deposited onto this. The TFHFG works by connecting it to a constant current power supply with copper tracks and wires. It is fed a constant current and the voltage signal over time is recorded. By choosing a suitable material for the TFHFG, the measured voltage can be correlated to surface temperature, by a calibration coefficient. In this campaign, platinum is used as material for the TFHFGs, since it has a linear change in voltage with temperature in the temperature range expected in the ITD.

Manufacture

The TFHFGs are manufactured in-house. Two individual black/transparent masks are designed and printed, with the copper tracks (transparent) on one and the platinum gauges (black) on the other. Figure. 4.2.9 shows an inverted mask of the copper tracks to TFHFGs at 10% height. The former mask is used to etch out the spacing between copper tracks from a copper clad polyimide sheet with the desired thickness of polyimide. The second mask is etched so that holes appear where the gauges are located. This is put on top of the copper tracks and platinum is deposited onto it, in the area where the gauges are to be located. When the second mask is removed, platinum is left only where desired.

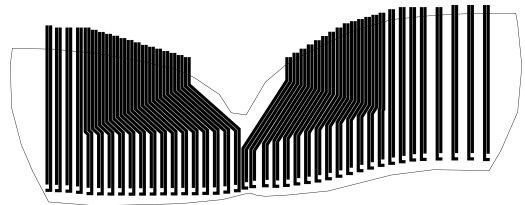


Figure 4.2.9: *Mask of the copper tracks for TFHFGs at 10% height*

The deposition of platinum is carried out with the sputter deposition technique. The

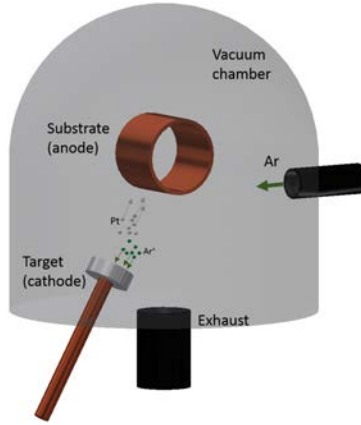


Figure 4.2.10: *Schematic of the method of sputter decomposition*

polyimide sheet with copper tracks and the second mask on top is fixed onto a revolving wheel (anode) situated inside a vacuum chamber. The air inside the chamber is evacuated and a magnetron is used to create a plasma of charged argon particles close to a target of platinum (cathode). Positively charged argon particles are attracted to the negatively biased platinum target at a very high velocity. The collision between the argon particles and platinum target creates a momentum transfer and ejects atomic sized platinum particles that travels to the revolving wheel with the polyimide sheet. A sketch covering the technique is see in Figure 4.2.10.

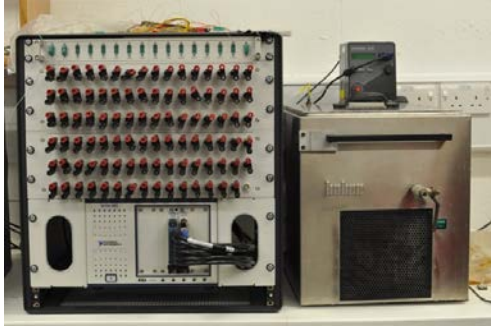
Annealing

With this manufacturing technique, where platinum is deposited onto the copper clad polyimide at low temperatures, the TFHFGs are unstable before going through an annealing process. Meaning that the TFHFG is not showing a desired relation between resistance and temperature, due to a variation in R_{in} over time. By cycling the TFHFG between an oven at $80\text{ }^{\circ}\text{C}$ and a freezer at $-20\text{ }^{\circ}\text{C}$ over a period of 3 days, its microstructure settles and the TFHFG is giving more accurate calibration.

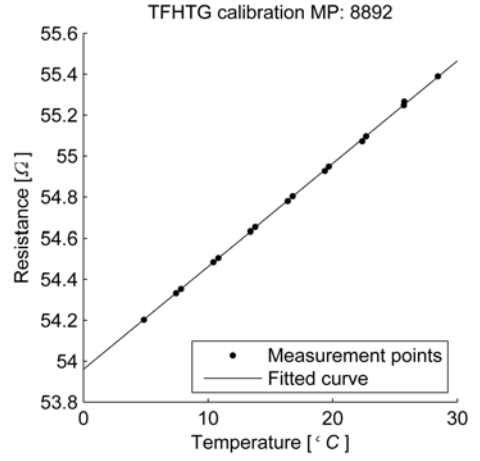
Calibration

The TFHFGs are calibrated in a fully automated water bath, see Figure 4.2.11a. Each TFHFG's resistance is measured at various temperatures, established by altering the temperature in the water bath. The temperature is measured both in the water and on the surface of the ITD vane, close to the TFHFGs, and a convergence criteria is set to determine when both the water and the gauge are experiencing the pre-set temperature. Eq. 4.2.1 shows the relation between temperature and resistance within a material.

$$R = R_{in} (1 + \alpha_{R/T} (T_w - T_{in})) \quad (4.2.1)$$



(a)



(b)

Figure 4.2.11: *The water bath and a typical calibration of a TFHFG*

If $T_{in} = 0$ °C, then R_{in} is the resistance at 0 °C, giving

$$R = \alpha_{R/T} R_{in} T_w + R_{in} \quad (4.2.2)$$

The temperature coefficient of resistivity, $\alpha_{R/T}$, is determined by a linear fit to the calibration data. An example of calibrating a TFHFG is included in Figure 4.2.11b.

Data processing

For each run in the OTRF the voltage applied to each individual gauge is recorded. To calculate the temperature signal based on the recorded voltage signal, Eq. 4.2.1 is rewritten with Ohms law, Eq. 4.2.3, which with a constant current is defined as Eq. 4.2.4. This gives Eq. 4.2.5 - 4.2.6, which when solved for the wall temperature gives Eq. 4.2.7. Hence, by recording the initial voltage over a gauge and temperature at the start of a run, along with the voltage signal over a run, the wall temperature history can be derived.

$$V = IR \quad (4.2.3)$$

$$V = I_{in} R \quad (4.2.4)$$

$$V = I_{in} R_{in} (1 + \alpha_{R/T} (T_w - T_{in})) \quad (4.2.5)$$

$$V = V_{in} (1 + \alpha_{R/T} (T_w - T_{in})) \quad (4.2.6)$$

$$T_w = \frac{V - V_{in}}{\alpha_{R/T} V_{in}} + T_{in} \quad (4.2.7)$$

To retrieve a heat transfer signal from the temperature signal, it is assumed that the penetration of the thermal pulse during a test is small, due to the short run time of the OTRF. The aluminium piece can therefore be assumed semi-infinite, and the one dimensional heat conduction equation, Eq. 4.2.8, is used to derive the heat transfer signal from the temperature signal. An impulse response filter is created with the same length as the sampled temperature signal. Using a known heat transfer signal (for example a step function) and its corresponding temperature signal, an impulse response function can be found by deconvolving Eq. 4.2.9. This function, $h_{Imp}[n]$, is then used to derive the heat transfer signal by convolving the calculated temperature signal as in Eq. 4.2.9. The impulse response filtering technique is in more detail described by Oldfield [41], who also compared it with previous techniques with great success.

$$\frac{\partial^2 T}{\partial x^2} = \frac{1}{\alpha} \frac{\partial T}{\partial t} \quad (4.2.8)$$

$$q[n] = h_{Imp}[n] * T[n] = \sum_{i=0}^{N-1} h_{Imp}[i] T[n-i] \quad (4.2.9)$$

Adiabatic wall temperature evaluation

To calculate the Nusselt number in Eq. 4.2.10 a reference temperature is needed. Ideally the adiabatic wall temperature, T_{aw} , can be evaluated.

$$\text{Nu} = \frac{q C_{ITDV}}{(T_{aw} - T_w) k} \quad (4.2.10)$$

When a measured wall temperature signal and corresponding heat flux signal exist, T_{aw} can be evaluated by fitting a linear regression to the convective heat flux equation in Eq. 4.2.11. The adiabatic wall temperature is found where the regression intersects $q = 0$.

$$q = h(T_w - T_{aw}) \quad (4.2.11)$$

As the temperature step on the ITD vane is low (10 – 20 degrees) the regression becomes inaccurate. Using the floating regression technique developed by Collins et al. [42], which utilizes data from multiple runs and compensates for changes in the inlet total temperature during a run, the accuracy of the regression is increased. The adiabatic wall temperature in Eq. 4.2.11 can be replaced with a linear function of the inlet total temperature, giving Eq. 4.2.12.

$$q = h(T_w - c_1 T_{01}) \quad (4.2.12)$$

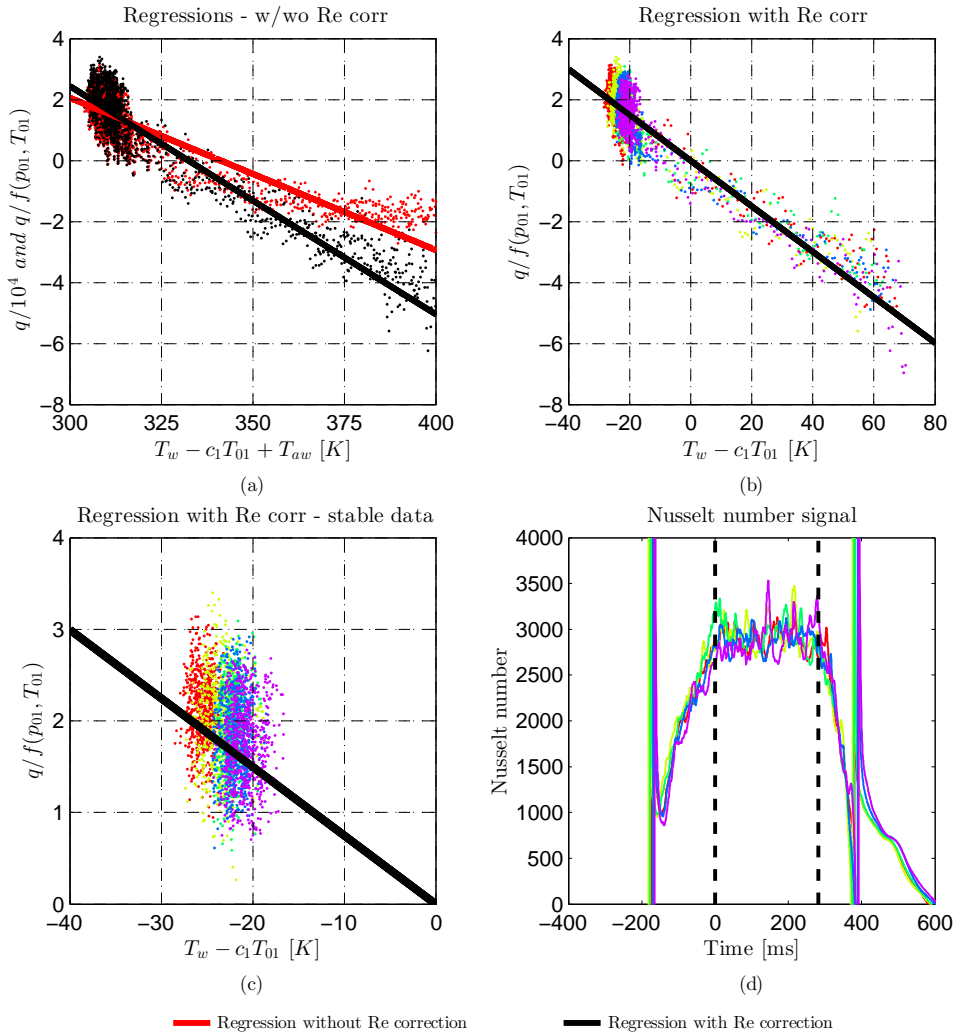


Figure 4.2.12: (a) Example of regression with and without the correction term for a single gauge and multiple runs. (b) Regression of data with the correction term for multiple runs individually coloured. (c) Regression with the correction term for multiple runs individually coloured with data only within the averaging time window. (d) Corresponding Nusselt number time signal with dashed lines indicating the extent of the averaging window.

A corrected wall temperature as in Eq. 4.2.13 can be determined and plotted against the heat flux signal. The adiabatic wall temperature is then defined as $c_1 \overline{T_{01}}$ and is given by the intercept with the corrected temperature axis.

$$T'_w = T_w - c_1 (T_{01} - \overline{T_{01}}) \quad (4.2.13)$$

The method was further refined by resampling the heat flux data at regular intervals of T'_w . Still, the method was not found to be fully applicable in these measurements with a small temperature step and to that relatively large fluctuations. An extension of the time window of data used was suggested, to utilize colder air that travels through the facility at the end of the run and hence extend the temperature range available for the regression. This extends the time window of data used past the aerodynamically stable part of the run where there is a change in Reynolds number. To account for this, a correction term is included based on turbulent flat plate theory where the Nusselt number is correlated with Reynolds and Prandtl number (Eq. 4.2.14).

$$\text{Nu} = \frac{hC_{ITDV}}{k} = c_2 \text{Re}^{4/5} \text{Pr}^{1/3} \quad (4.2.14)$$

By re-writing Eq. 4.2.14 such that h is a function of p_{01} and T_{01} the convective heat transfer equation in Eq. 4.2.12 becomes Eq. 4.2.15.

$$\frac{q}{f(p_{01}, T_{01})} = c_3 (T_w - c_1 T_{01}) \quad (4.2.15)$$

Figure 4.2.12 show an example of the floating regression technique with and without the correction term applied on data from a single gauge and multiple runs. The resulting Nusselt number signal is included to highlight the small variation between runs.

4.2.3 Probe

A three-hole probe with two thermocouples has been designed, manufactured and calibrated, to be traversed at the exit of the ITD. When used in the OTRF, the probe is mounted in a carriage monitored by a Linear Variable Differential Transformer (LVDT) and traversed 1.5 ITD vane pitches. For each run, a single height will be traversed, travelling in the same direction as the rotor. Figure 4.2.13 shows a photo of the probe and the probe mounted in the calibration tunnel. The probe consists of five steel pipes ($\varnothing 1.6$ mm), out of which three constitute the pressure probe and the remaining two accommodate a 0.0254 mm K-type thermocouple each. Different mounts have been manufactured, to hold the probe in the calibration tunnel and OTRF. Scanivalve tubes are attached to the aft of the probe to carry the pressure measurements outside of the facility to pressure transducers, together with the thermocouple wires.

Calibration

The three-hole probe was calibrated in the in-house 9" – by – 3" facility, which has been used for similar calibrations before. It is a partially-closed-loop ejector driven transonic wind tunnel. The facility's name stems from the simple fact that the test section

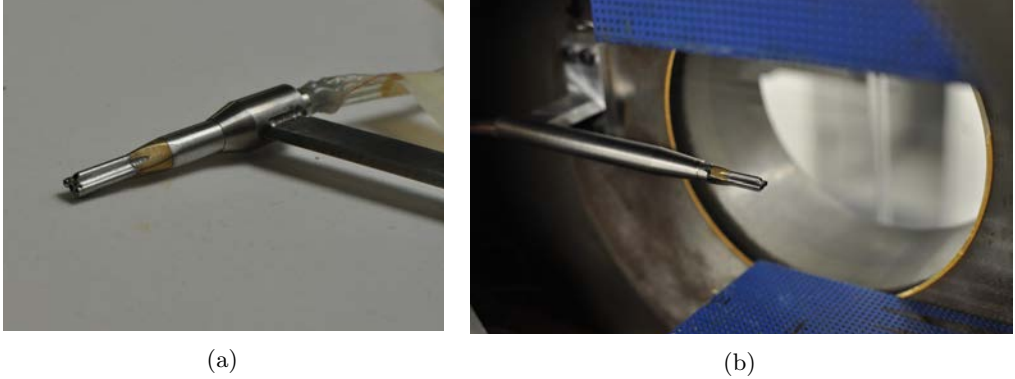


Figure 4.2.13: (a) *Three-hole probe with two thermocouples.* (b) *Probe mounted in the calibration tunnel.*

size is 9 inch by 3 inch. The height of the test section is however variable, and a two dimensional perforated nozzle was used in this calibration. The total pressure within the facility is measured with a Pitot probe upstream of the inlet contraction. Static pressure measurements were taken on the sidewall at the axial position of the probe tip, as well as 10 mm up- and downstream. The probe was calibrated in the range of ± 20 degrees, with steps of 0.5 degrees, in the yaw plane and M between 0.2 – 1.2. Since it is a three-hole probe it was only calibrated for a single pitch angle, 0 degrees, although spot checks were performed at other angles to determine its sensitivity. The yaw angle was changed in between runs by manually turning the probe in situ. The M was altered during a run, by partially closing a valve regulating the mass flow through the tunnel. For a run to be considered acceptable, enough time must be left in between closing the valve for the M to become steady.

The analysis of the acquired calibration data is performed using the non-dimensional parameters defined in Eq. 4.2.16 - Eq. 4.2.19, stated in Povey et al. [43] and Main et al. [44]. The fact that the parameters are non-dimensional provides that the calibration is independent on the total pressure, p_{01} , in the facility, which is necessary since it is significantly lower in the 9" – by – 3" than in the OTRF. The acquired data is gathered in a calibration matrix, that simply works as a look-up table, to which measurements will be compared to determine the measured M and flow angle. Figure 4.2.14a shows the distribution of C_β within the range of M and yaw angles the probe is calibrated. The calibration is shown to be fairly smooth, except for an area at low M and high positive yaw angles where a sudden drop is visible, from the otherwise smooth plane. A number of repeat runs were conducted for these points with unchanged results, giving that it is likely to be due to a slight asymmetry of the probe.

$$C_\beta = \frac{p_a - p_c}{p_b - p_{avg}} \quad (4.2.16)$$

$$C_{p_0} = \frac{p_{01} - p_b}{p_b - p_{avg}} \quad (4.2.17)$$

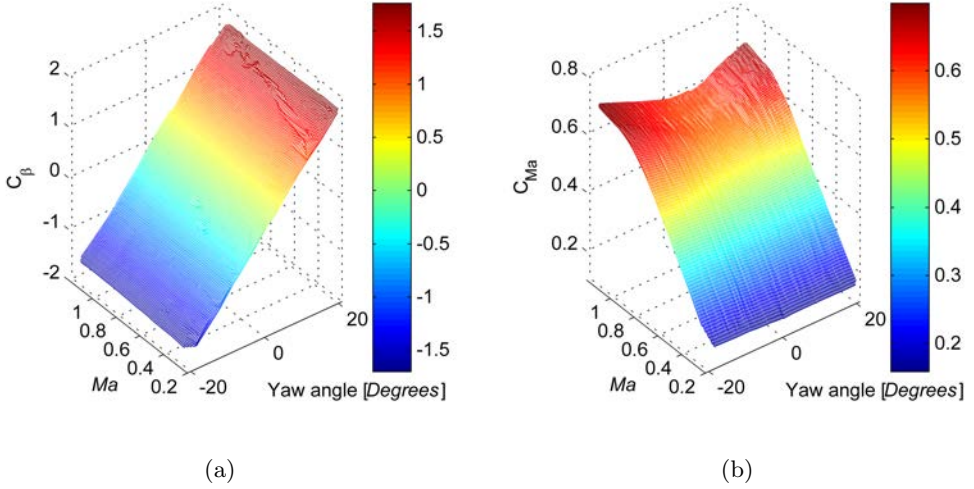


Figure 4.2.14: Results from calibrating the three-hole probe. Distribution of C_β (a) and C_M (b) over the ranges of yaw angles and M calibrated within.

$$C_M = \sqrt{\frac{2}{\gamma - 1} \left[\left(\frac{p_{avg}}{p_b} \right)^{\frac{1-\gamma}{\gamma}} - 1 \right]} \quad (4.2.18)$$

$$p_{avg} = \frac{p_a + p_c}{2} \quad (4.2.19)$$

The calibration data is transformed into a "look-up" application matrix used to reconstruct the measured pressures into yaw angle, M and P_0 (see Main et al. [44]).

4.2.4 Other Instrumentation

Other than the instrumentation mentioned above, this configuration has also been equipped with Pitot probes at the leading edge of one ITD vane at five different heights (15, 25, 50, 75 and 90%) to measure the total pressure into the ITD. There are also total pressure/temperature rakes positioned at the exit of the duct at five circumferential locations covering two ITD vane pitches (30 degrees). Each rake consists of eleven Pitot probes/thermocouples equidistant between the hub and shroud.

4.2.5 Acquisition System

To record the measured data, the following acquisition set-up has been used:

- Pressure measurements: National Instruments 6225 M series data acquisition system and Sensor Technics CTE8000 series pressure transducers.

- Low speed TFHFG: National Instruments 6225 M series data acquisition system and HTA3 amplifier manufactured by Monitron.
- Thermocouples: National Instruments 6225 M series data acquisition system and National Instruments TC 2095 cold junction compensator.
- Traverse system: Pneumatic actuator and a LVDT.

4.2.6 Uncertainty

There are several sources of uncertainty that contribute to the overall uncertainties in measurements, both directly measured and derived quantities. These can be divided into two groups of errors, bias and precision. Bias errors are systematic and gives a fixed error which remains constant during a test. Precision errors are random and are often assumed to be Gaussian in distribution. Individual sources of Bias (B_k) and Precision (S_k) errors affecting a measured quantity are combined as in Eq. 4.2.20 and Eq. 4.2.20.

$$B_x = \sqrt{B_1^2 + B_2^2 + \dots + B_k^2} \quad (4.2.20)$$

$$S_x = \sqrt{S_1^2 + S_2^2 + \dots + S_k^2} \quad (4.2.21)$$

As precision error often are assumed to be Gaussian in distribution the standard deviation (σ), a measure of its variation from the sample mean, can be determined. For an infinite number of measurements it is defined by Eq. 4.2.22.

$$\sigma = \sqrt{\frac{1}{N} \sum_{i=1}^N (x_i - \bar{x})^2} \quad (4.2.22)$$

However, in most experiments there are a limited number of measurements due to limitations in time and financial resources. The standard deviation is then defined by Eq. 4.2.23.

$$\sigma_x = \sqrt{\frac{1}{N-1} \sum_{i=1}^N (x_i - \bar{x})^2} \quad (4.2.23)$$

The bias and precision errors can be combined to provide an overall uncertainty in the measurement. Typically a 95% confidence interval is used for the precision errors, corresponding to the value being within two standard deviations (2σ). The overall uncertainty of a parameter is defined by Eq. 4.2.24.

$$U_x^{95\%} = \sqrt{B_x^2 + (2\sigma_x)^2} \quad (4.2.24)$$

Table 4.2.1: Uncertainties for heat transfer independent parameters

Parameter	Nominal value	Uncertainty
Ambient temperature	295 K	$\pm 0.5\%$
Thin film gauge measured voltage (ΔV)	3.5 mV	$\pm 1.0\%$
Constant current supply for thin film gauges (I)	5 mA	$\pm 0.4\%$
Gauge resistance at 0°C (R_0) obtained during calibration	50 Ω	$\pm 0.2\%$
Gauge thermal coefficient of resistance (α) obtained during calibration	$1 \times 10^{-3} \text{ VK}^{-1}$	$\pm 2.5\%$
$\sqrt{\rho c k}$ for the gauge substrate	569 $\text{Jm}^{-2}\text{K}^{-1}\text{s}^{1/2}$	$\pm 4\%$

Table 4.2.2: Uncertainties for heat transfer derived parameters

Parameter	Nominal value	Uncertainty
Temperature rise (ΔT)	15 K	$\pm 2.70\%$
Wall temperature (T_w)	310 K	$\pm 0.49\%$
Heat flux (q)	$2.2 \times 10^4 \text{ Wm}^{-2}$	$\pm 4.72\%$
Heat transfer driving temperature ($T_{aw} - T_w$)	30 K	$\pm 5.88\%$
Nussel number (Nu)	3000	$\pm 7.54\%$

The uncertainties of individual parameters propagate through to any parameter derived from them. The uncertainty of a derived parameter P can be obtained from the independently measured parameters x, y, z by Eq. 4.2.25.

$$\sigma_P = \left[\left(\frac{\partial P}{\partial x} \right)^2 \sigma_x^2 + \left(\frac{\partial P}{\partial y} \right)^2 \sigma_y^2 + \left(\frac{\partial P}{\partial z} \right)^2 \sigma_z^2 \right]^{1/2} \quad (4.2.25)$$

The overall uncertainties associated with the heat transfer measurements are presented in Table. 4.2.1 and 4.2.2.

Uncertainties in the pressure measurements stem from the acquisition system. The OTRF uses CTE8000 series pressure transducers from Sensor Technics. The transducers are calibrated in-house using a Ruska model 7250 gauge digital pressure controller (DPC)

Table 4.2.3: Uncertainties in pressure measurements

Error source	Quoted or estimated error	Uncertainty
Sensor Technics CTE8000 pressure transducers, Quoted accuracy	$\pm 0.1\%$	$\pm 0.1\%$
Transducers calibration accuracy (Ruska DPC, Beard [45])	$\pm 0.019\%$	$\pm 0.019\%$
National instruments 6225 M Series data acquisition card, Quoted accuracy	$\pm 3100 \mu V$	$\pm 0.031\%$
Overall uncertainty in pressure measurements		$\pm 0.11\%$

Table 4.2.4: Uncertainties in 3-hole probe calibration

Parameter	Uncertainty
Yaw angle	$\pm 0.16^\circ$
Mach number	± 0.017
Total pressure	$\pm 0.067\%$

and the data is recorded using National instrument 6225 M series data acquisition cards. The uncertainties associated with the transducers, their calibration, and data acquisition system are provided in Table. 4.2.3. The measurements are also affected by the length of the scanivalve tubing. Efforts were taken to reduce its length. Beard [45] performed an extensive analysis for the conditions in the OTRF and concluded in a total magnitude error of 0.084% when using a 0.3 m long scanivalve tube, typical also in this test campaign.

The probe uncertainty was evaluated by comparing data from the calibration tunnel to that calculated by processing the data using the determined application matrix. The measured values were subtracted from the calculated to determine the error in each calibration point. The probe uncertainty to 95% confidence was calculated from the standard deviations of the differences between the data. The evaluated uncertainties are presented in Table. 4.2.4 to 95% confidence. Uncertainties in the pressure measurements are presented in Table.4.2.3 and discussed above.

5 CFD methodology

Throughout the thesis results from CFD are included, both for comparison with the experimental results and as a tool to further explain the flow through the ITD and its effect on the heat transfer. ANSYS CFX was used for all predictions and meshes were created using ICEM CFD or a GKN in-house software (G3Dmesh, during the design of the FACTOR ITD). It should be noted that the CFD performed is not aiming at pushing any boundaries in the development of better tools, but rather be representative of conventional tools used in industry today. Table 5.0.1 lists the different predictions performed throughout this project, by me and others.

Predictions of the NFFP5 geometry were performed by GKN Aerospace Engine Systems. The CFD was set-up with the ITD on its own and measured tangentially averaged profiles of total pressure and flow angles at the inlet and a mass flow at the exit. CFD predictions were performed for the on-design case only. The results were included in Johansson et al. [46].

Different set-ups have been used to predict the flow through the FACTOR geometry. Ahead of designing the ITD, a throughflow calculation was performed by Rolls-Royce Plc using their in-house code Q263. The results were used as targets in the design phase along with geometric targets and restrictions. GKN Aerospace Engine Systems in-house code VolVane was used to generate designs and ANSYS CFX version 12.1 was used to evaluate each design. Results were evaluated and compared with targets and used by the designer as input when generating the next geometry. Pre-test steady CFD of the final design was performed of the ITD on its own and of the ITD together with the HPT stage. Meridional views of the domains used are seen in Figure 5.0.1b and Figure 5.0.1a, respectively. Results were compared with experimental results during commissioning of the facility, to find its operating point. A comparison was made with initial results from the Uniform test campaign. A pre-test unsteady prediction of the 1.5 stage was performed to support instrumentation. The results were included in Johansson et al. [47].

Post-test CFD analysis performed using ANSYS CFD version 15.0 utilized the measured ITD exit endwall static pressure to create a linear radial profile set as the exit boundary condition. Steady predictions of the ITD only domain and the 1.5 stage domain (see Figure 5.0.1b and Figure 5.0.1a) were performed and compared with experimental results from the Uniform test campaign. Flow visualization such as surface streamlines showed large radial flow migration near the surface of the ITD vane affecting the adiabatic wall temperature distribution along the vane. The 2-dimensional distribution lead to further investigations of how to determine the experimental adiabatic wall temperature as discussed in section 4.2.2. The results were included in Johansson et al. [48].

Further CFD was performed using ANSYS CFX version 16.0 where a 90-degree domain of the 1.5 stage FACTOR geometry (see Figure 5.0.1a and Figure 5.0.2) was set-up to perform unsteady analysis. The HPT vane - HPT blade - ITD vane count for the FACTOR configuration is 32-60-24, and its periodicity 8-15-6, hence a 90-degree sector was needed to perform a full unsteady prediction. With a 90-degree sector domain the model quickly becomes large, and hence efforts were taken to keep the overall mesh size down. Automatic wall functions were used throughout the whole domain and the mesh was set-up such that wall functions were activated in the HPT vane and rotor domain

while the boundary layer flow is modelled in the ITD domain (with a y^+ value kept below 0.7). Predictions were performed for all three inlet conditions to the HPT stage; Uniform, Swirl 1, and Swirl 2. In an effort to better match the ITD vane surface static pressure measurements numerous attempts were made, by changing the exit boundary condition, without significant improvement. Attempts were also made by extending and shortening the ITD domain without significant improvement. The results presented in Johansson et al. [49]-[50] uses an average static pressure at the exit of the ITD, allowing for spanwise and tangential variation.

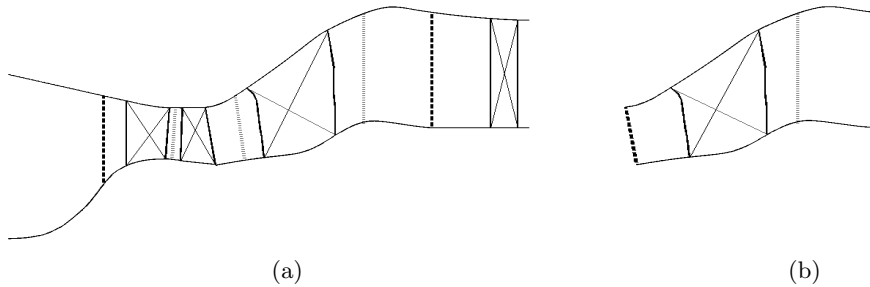


Figure 5.0.1: *Meridional view of the HPT stage, ITD and Deswirl (a) and of the ITD only domain (b). The dashed lines show the location of domain inlet and outlet. The dotted lines indicate the HPT vane, HPT rotor and ITD vane exit planes.*

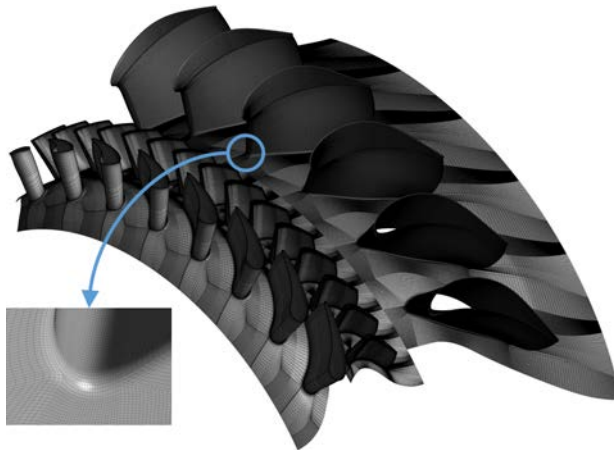


Figure 5.0.2: *Unsteady CFD domain with mesh lines along hub and vane/blade surfaces. Also zoomed in on the ITD vane leading edge/hub region.*

Table 5.0.1: Summary of CFD set-ups included in Johansson et al [46]-[50]

Code	Geometry	Simulation	Boundary conditions	Purpose
CFX v.12.1	NFFP5	ITD only	Radial profiles at inlet and a massflow at outlet	Comparison with experiments
Q263	FACTOR	Throughflow	Homogenous	Provide targets for ITD design
VolVane	FACTOR	ITD only 3D Euler	Radial profiles	Design ITD
CFX v.12.1	FACTOR	ITD only	Radial profiles	Evaluate design of ITD and comparison in commissioning and with initial data
CFX v.12.1	FACTOR	1.5 stage unsteady	Homogeneous inlet and radial profile at outlet	Support instrumentation
CFX v.12.1	FACTOR	1.5 stage steady	Homogeneous inlet and radial profile at outlet	Comparison in commissioning and with initial data
CFX v.15.0	FACTOR	ITD only	Radial profiles	Comparison with Uniform data
CFX v.15.0	FACTOR	1.5 stage steady	Homogeneous inlet and radial profile at outlet	Comparison with Uniform data
CFX v.16.0	FACTOR	1.5 stage unsteady - Uniform	Homogeneous inlet and averaged static pressure at outlet	Comparison with data from multiple inlet conditions
CFX v.16.0	FACTOR	1.5 stage unsteady - Swirl 1	Velocity vectors at inlet and averaged static pressure at outlet	Comparison with data from multiple inlet conditions
CFX v.16.0	FACTOR	1.5 stage unsteady - Swirl 2	Velocity vectors at inlet and averaged static pressure at outlet	Comparison with data from multiple inlet conditions

6 Lessons Learned

This chapter presents lessons learnt throughout the project that can be included and implemented in future projects. This includes instrumentation that would have eased the data analysis as well as improvements in the measurement techniques used.

To increase the accuracy of the measurements of initial wall temperature, thermocouples could have been placed on the surface of the ITD vane, near the TFHFGs, and measurements taken before the start of each run. Total temperature measurements at the rotor exit, either conducted with a T_0 rake or through a full area traverse would be useful as a guide to the levels of adiabatic wall temperatures expected on the ITD vane. A full area traverse of total temperature and aerodynamics would be useful to further explain the intensity of the vane-to-vane clocking effect, the changes in incidence between adjacent vanes due to the clocking effect and with change in HPT stage inlet condition, and to validate predictions of the HPT stage.

To increase the accuracy of the regression of wall temperature and heat flux data, a data set with larger difference in initial temperature would be beneficial. This could for example be achieved by heating or cooling the ITD vane to a controlled temperature ahead of a run. In a configuration such as this, it is limited to accessibility in the rig due to the number of vanes instrumented with TFHFGs. Also, the thickness of the insulating Kapton layer could be increased to reduce the conduction into the aluminium. Another measurement technique that is currently being implemented in the OTRF is to use a double sided gauge, where the temperature is also measured in between the first insulating layer and the second layer.

Due to limitations in the total mesh size, a rather coarse mesh was used in the HPT stage in the unsteady CFD, utilizing automatic wall functions instead of modelling the boundary layer. A finer mesh would perhaps predict a slightly different HPT rotor exit condition, specifically in the HPT rotor tip leakage area which involves significant secondary flows and large gradients. Coming projects in the OTRF are designed with a more "CFD-friendly" vane-blade-vane count allowing for reasonable computational times with a finer mesh.

Efforts are made to avoid problems faced in this project in coming projects in the OTRF.

7 Summary of papers

This chapter includes summaries of the appended papers, some comments about their results and my contributions to each of them.

7.1 Paper A

Experimental and Numerical Investigation of an Aerodynamically Loaded Guide Vane in a Turbine Duct

7.1.1 Summary

The first appended paper describes a re-build of the Chalmers LSLS Turbine Facility in which a new ITD and its low turning vane was installed. The configuration is representative for a counter-rotating engine design. Experimental data of ITD vane surface static pressure at five heights (5, 25, 50, 75, and 95%) are included. A 7-hole pressure probe was traversed at the ITD inlet and exit plane, covering an ITD vane passage. Experiments were conducted with three inlet conditions to the ITD, with different swirl angles achieved by varying the HPT rotor speed. The experimental data is compared with steady CFD results performed with the ITD on its own and on-design inlet condition. The ITD inlet measurements show a non-uniform flow field with traces of secondary flows from the upstream HPT vane. The change in ITD inlet swirl angle is seen to affect the early part of the vane with changes in vane loading. The CFD results is found to match the experimental ITD vane static pressure distribution fairly well, although a tip leakage vortex roll-up on the pressure side is seen to locally lower the static pressure which is not seen in the experimental data. The ITD vane is seen to turn the flow to the same swirl angle profile at the ITD exit, proving it to be robust to changes in the inlet condition. Contours of total pressure from CFD at the ITD exit show the HPT rotor tip leakage vortex to end up roughly mid passage in both the tangential and radial direction, further visualized by streamlines. This is not seen in the experimental data and sensitivity studies of the CFD inlet condition in the tip leakage region shows influence on the predicted vortex structure and the outlet plane total pressure loss regions.

7.1.2 Comments

I contributed by participating in the experimental measurements and analysis of the experimental results. I was also the main contributor to writing the paper.

7.2 Paper B

Aerodynamic and Heat Transfer Measurements on an Intermediate Turbine Duct Vane

7.2.1 Summary

The second appended paper describes the design, instrumentation, commissioning, and installation of an ITD with its medium turning vane in the OTRF. A throughflow model was set-up by Rolls-Royce Plc and results were used to set targets in the design stage, along with geometrical targets and constraints. The final design was found to meet these targets. Pre-test unsteady CFD showed an interaction between the HPT vane and ITD vane due to the vane count between the two (32 HPT vanes to 24 ITD vanes). To investigate this in the experiments, three adjacent vanes were instrumented in an identical manner. This included static pressure tappings, thin film heat flux gauges on the ITD surfaces, and a 3-hole pressure probe equipped with two thermocouples traversed at the ITD exit. Experimental results presented include commissioning results, ITD vane static pressure at three radial heights and ITD vane Nusselt number. The experimental results were compared with pre-test steady ITD only and 1.5 stage CFD. The ITD vane static pressure measurements showed the clocking effect to be largest at 10% height due to stronger HPT vane secondary flows transported through the HPT rotor. Nusselt numbers were presented at 50% height. CFD predictions included are found to perform fairly well, although the Design CFD has difficulties predicting the 90% static pressure profile, believed to be due to differences in the tip leakage flow between the boundary condition used and the experiments. The CFD is also seen to highly under-predict the heat transfer along the pressure side of the ITD vane.

7.2.2 Comments

The heat transfer measurements were evaluated using mean HPT rotor exit total temperature corrected with the recovery factor, based on the pressure measurements. As the flow near the surface of the ITD vane migrates radially, this is not an adequate way to determine the adiabatic wall temperature around the ITD vane. A different evaluation method was developed to the next paper. Past the publishing of this paper, some of the gauges along the suction side were found to be delaminated and hence providing unreasonable results (seen as spikes between 25 and 50 mm surface distance on ITD vane 1 and 3).

My contribution consisted of:

- 3D CFD evaluation of each individual ITD design.
- Design and calibration (when necessary) of TFHFGs, pressure tappings, three-hole probe, rakes.
- Evaluation of measurements to determine the operating point.
- Evaluation of measurements.

The manufacture of hardware and instrumentation has been performed by technicians at University of Oxford and externally. The running of the OTRF and data acquisition is performed by test engineers. I was the main contributor to writing the paper.

7.3 Paper C

Aerothermal Measurements and Predictions of an Intermediate Turbine Duct Turning Vane

7.3.1 Summary

The third paper presents further results from the Uniform measurement campaign. Nusselt numbers along three radial heights and on the casing just upstream of the ITD vane are included. A 3-hole pressure probe with thermocouples mounted above and below was traversed at the ITD vane exit. Contours and tangentially averaged profiles of p_{03} , M , whirl angle, and T_{03} are presented. Experimental data are compared with results from two steady post-test CFD predictions, a ITD only and a full 1.5 stage configuration. There is a discussion on how to evaluate the adiabatic wall temperature needed to reduce the heat transfer measurements to Nusselt number. With significant radial flow migration along the ITD vane surface seen in the CFD results a simple 2D approach using a fixed T_{03} and a recovery effect is not suitable in this case. Using a linear regression to the T_w and q data, the adiabatic wall temperature is found where the regression intersects $q = 0$. With the small wall temperature rise seen on the ITD vane during a run, an extension of the time window of data used was necessary to utilize colder air travelling through the facility and thus extend the temperature range available for the regression. A correction term was included to compensate for the change in Re . The results showed a larger clocking effect in Nusselt number along the 10% height, common with the static pressure results included in Paper B. The CFD results is seen to under-predict the Nusselt number on the ITD vane pressure side at the 10 and 50% heights while largely over-predicting it at 90% height. The over-prediction at 90% is connected to the complexity in predicting the HPT rotor tip leakage flow. The heat transfer is highly influenced by the intensity of the secondary flow and its flow angle.

7.3.2 Comments

Nusselt number results on the very late suction side at 50% height is seen to continue dropping towards the trailing edge, while flattening out in the CFD. This is connected to the quickly increasing experimental T_{aw} in this region. Different explanations to this is brought up in the paper. Some increase in T_{aw} is expected due to the deceleration past the ITD vane throat. Possible further explanations include the warmer tip leakage fluid migrating radially inwards and reaching the late 50% height, and as the vane is relatively thin near the trailing edge the 1D heat transfer assumption might not be accurate.

My contribution consisted of analysing the experimental data, partly analysing the CFD, and being the main contributor to writing the paper.

7.4 Paper D

Effect of Low-NO_x Combustor Swirl Clocking on ITD Vane Aerodynamics with an Upstream HPT Stage - an Experimental and Computational Study

7.4.1 Summary

The forth paper include aerodynamic results for three different inlet conditions to the HPT stage: Uniform and two low-NO_x swirl profiles. Experimental data taken with static pressure tappings on the ITD vane and a 3-hole pressure probe traversed at the ITD exit are compared with results from unsteady CFD predictions performed with all three inlet conditions. Changes in the aerodynamics through the HPT stage with the Swirl conditions is discussed based on results from the unsteady predictions. The Swirl conditions are seen to change the location of the stagnation point and the loading along the early HPT vane. It also influences the boundary layer flow of the HPT vane, leading to increased total pressure losses near the endwalls and changes in the HPT vane exit whirl angle profile. With a reduction in HPT vane capacity an increase in the M is noted. Total pressure contours at the HPT rotor exit clearly show the clocking effect as areas of lower total pressure, aligned with where the HPT vane secondary flow ends up. The Swirl conditions are seen to tilt the radial distribution of the HPT vane secondary flows at the HPT rotor exit. Experimental results of static pressure along the ITD vane show the 10% height to be most influenced by the clocking effect, for all three inlet conditions. ITD vane 2 is seen to be the vane most influenced by changing inlet condition, as its leading edge is aligned with HPT vane secondary flows existing the HPT rotor. A change in incidence to the vane is seen, affecting the acceleration along the early parts of the vane. CFD results show the fluctuations in static pressure to be largest at 10%. Overall, the clocking effect is seen to have larger effect on the ITD vane static pressure than changing the inlet condition, seen both in experimental data and CFD results. Experimental contours and radial profiles at the ITD exit show a drop in p_{03} and M with the Swirl conditions. CFD results are seen to not be able to predict the radial distribution of p_{03} and M. Prediction of the whirl angle show larger radial variation compared to the experimental data. The larger whirl angles at 40 – 80% height (depending on inlet condition) is flow originating from the HPT rotor secondary flow.

7.4.2 Comments

The CFD is seen to have difficulties in predicting the radial pressure gradient in the ITD. This is noted comparing the data from ITD vane static pressure and ITD exit profiles. Numerous attempts were made, by changing the exit boundary condition, without significant improvement. It should be noted that efforts were made to reduce the mesh size in the HPT stage, to keep the overall mesh size and computational times down. This was necessary as the periodicity of the current configuration is 90 degrees.

I contributed by analysing the experimental data, performing and analysing the CFD, and being the main contributor to writing the paper.

7.5 Paper E

Effect of Low-NO_x Combustor Swirl Clocking on ITD Vane Heat Transfer with an Upstream HPT Stage - an Experimental and Computational Study

7.5.1 Summary

The fifth paper include heat transfer results for three different inlet conditions to the HPT stage: Uniform and two low-NO_x swirl profiles. Experimental data taken with thin film heat transfer gauges on the ITD vane surface and a 3-hole pressure probe equipped with thermocouples above and below traversed at the ITD exit are compared with results from unsteady CFD predictions conducted with all three inlet conditions. Changes in the total temperature field through the HPT stage with the Swirl conditions is discussed based on results from the unsteady predictions. The inlet swirl is seen to reduce the total temperature near the endwalls at the HPT vane exit due to increased losses. The radial profile at the HPT rotor exit is dominated by the higher temperature tip leakage flow. Both experimental data and CFD results show a re-distribution of the total temperature field through the ITD, as the tip leakage flow is mixed out with the main flow. Contours of T_{03} at the HPT rotor exit clearly show the clocking effect as areas of lower T_{03} , aligned with where the HPT vane secondary flow ends up. The flow coming off the pressure side of the ITD vane is seen to have a higher T_{03} . The T_{aw} distribution on the ITD vane is described. Radial inwards migration of warmer tip leakage fluid is noted along the vane surface, especially along the pressure side. A comparison of the experimentally evaluated T_{aw} and time averaged results from CFD show similarities in distribution, although the variation between gauges is seen to be larger in the experimental data, especially at 90%. Maximum and minimum envelopes show the time variation in Nusselt number to largest at 10%. The Nusselt number distribution on the ITD vane is not seen to be significantly different with the change in inlet condition. The CFD results is seen to match the experimental data well, although difference are seen at the late suction side at 50% due to reasons discussed in Paper C, and on the 90% pressure side where CFD is largely over-predicting the Nusselt number. Experimental data of Nusselt number on the casing upstream of the ITD vane are included and seen to be higher than along the ITD vane surfaces. A comparison of averaged time averaged unsteady CFD results from three adjacent vanes are compared with the results from steady CFD show them to provide similar results.

7.5.2 Comments

It should be noted that efforts were made to reduce the mesh size in the HPT stage, to keep the overall mesh size and run-times down. This was necessary as the periodicity of the current configuration is 90 degrees. The result of comparing unsteady and steady CFD is of particular interest as the cost is significantly increased for running unsteady CFD in this case. However, the clocking effect cannot be modelled with steady CFD. Of interest, is the results presented in this paper, showing an increase in Nusselt number on the ITD vane compared to that presented by Povey et al. [34], where a high turning ITD

vane in a co-rotating configuration with the same HPT stage was studied.

I contributed by analysing the experimental results, performing and analysing the CFD, and being the main contributor to writing the paper.

8 Concluding remarks

This thesis focuses on the aerothermal flow through an intermediate turbine duct, mainly conducted through experiments in two different facilities. CFD predictions are included as comparison and to further explain the aerothermal flow.

A new ITD configuration with a low turning vane was installed in the Chalmers LSLS Turbine Facility and aerodynamic measurements, including ITD vane static pressure distributions and area mappings of the swirl angle, total pressure and velocity upstream and downstream of the vane. The experiments were conducted with three different ITD inlet conditions, with varying swirl angle. The results proved the design to be robust in terms of delivering a similar flow at the outlet of the ITD, independent of the inlet swirl angle. The ITD vane loading is seen to be affected along the early parts of the vane by the change in incidence. Loss regions and difficulties in predicting the tip gap flow is discussed. A fairly good agreement was found with the CFD predictions with areas of misalignment connected to the prediction of the tip leakage vortex roll-up along the ITD vane pressure side.

A new ITD configuration with a low turning vane was designed, manufactured, instrumented, and installed in the OTRF. An extensive amount of instrumentation was designed, manufactured and installed. This thesis includes data from three measurement campaigns with different HPT stage inlet conditions; a uniform inlet flow and two low-NO_x swirl profiles (different clocking positions relative to the HPT vane). Results include static pressure and Nusselt number distributions on the ITD vane and aerothermal area traverse data at the ITD exit, presented as contours and radial profiles. Additional results include ITD endwall static pressure, and ITD exit total pressure and temperature taken with fixed rakes. Experimental results are compared with steady and unsteady CFD performed with an ITD only and a 1.5 stage configuration.

As the wall temperature rise during a run is rather small, there were difficulties in performing a regression to find the adiabatic wall temperature. The floating regression technique was used with an extension of the time window of data used. To compensate for the change in Reynolds number, a correction term was applied.

Results show the vane-to-vane clocking effect, due to the difference in vane count between the two vanes (32 HPT vanes and 24 ITD vanes), to change the incidence to the ITD vane, the static pressure level around it, and to a smaller degree also the Nusselt number distribution. The change in inlet condition is seen to have local effects in the ITD, as there is a slight shift in the location of where HPT vane secondary flows end up. It is however noted that the clocking effect is seen to have a larger effect on the ITD vane static pressure and Nusselt number distribution than the introduction of a low-NO_x swirl profile at the inlet to the HPT stage, which is seen in both the experimental data and the CFD results. The CFD is in general seen to be able to match the experimental data fairly well, although there is a difficulty in predicting the radial static pressure gradient through the ITD. Numerous attempts were made to better this, by changing the exit boundary condition, without significant improvement. A comparison of the Nusselt number from steady CFD with a time average of three adjacent ITD vanes taken from unsteady CFD is shown to provide similar results. This is of particular interest as the cost is significantly increased for running unsteady CFD in this case. However, the clocking effect cannot be

modelled with steady CFD.

It is also noted that the general flow field through the ITD is similar in both facilities, largely influenced by the upstream HPT stage secondary flows. The two facilities provide different opportunities and depending on the scope and budget of a project either or will be of interest.

Bibliography

- [1] E. Göttlich, A. Marn, F. Malzacher, and F. Heitmeir, "On flow separation in a super-aggressive intermediate turbine duct," in *Proceedings 8th European conference on turbomachinery fluid dynamics and thermodynamics*, 2009.
- [2] <http://www.strutpatent.com/patent/08061980/separation-resistant-inlet-duct-for-mid-turbine-frames#!prettyPhoto>. Accessed 9-January-2014.
- [3] R. G. Dominy and D. A. Kirkham, "The influence of blade wakes on the performance of intermediate diffusers," *Journal of turbomachinery*, vol. 118, no. 2, pp. 347–352, 1996.
- [4] R. G. Dominy, D. A. Kirkham, and A. D. Smith, "Flow development through interturbine diffusers," *Journal of turbomachinery*, vol. 120, no. 2, pp. 298–304, 1998.
- [5] G. Norris and R. Dominy, "Diffusion rate influences on inter-turbine diffusers," *Proceedings of the Institution of Mechanical Engineers, Part A: Journal of Power and Energy*, vol. 211, no. 3, pp. 235–242, 1997.
- [6] G. Norris, *Flows through s-shaped annular, inter-turbine diffusers*. Durham Theses, Durham University, 1998. Available at Durham E-Theses Online: <http://etheses.dur.ac.uk/760/>.
- [7] S. Hu, Y. Zhang, X. F. Zhang, and E. Vlasic, "Influences of inlet swirl distributions on an inter-turbine duct part I: Casing swirl variation," in *Proceedings of ASME Turbo Expo*, ASME, 2011. GT2011-45554.
- [8] Y. Zhang, S. Hu, X. F. Zhang, and E. Vlasic, "Influences of inlet swirl distributions on an inter-turbine duct part II: Hub swirl variation," in *Proceedings of ASME Turbo Expo*, ASME, 2011. GT2011-45555.
- [9] L.-U. Axelsson, *Experimental investigation of the flow field in an aggressive intermediate turbine duct*. PhD Thesis, Chalmers University of Technology, 2009.
- [10] C. Arroyo Osso, *Aerothermal investigation of an intermediate turbine duct*. PhD Thesis, Chalmers University of Technology, 2009.
- [11] L.-U. Axelsson and T. G. Johansson, "Evaluation of the flow in an intermediate turbine duct at off-design conditions," in *ICAS 2008, 26th international congress of the aeronautical sciences, Alaska, August 2008*, 2008.
- [12] C. Arroyo Osso, F. Wallin, and T. G. Johansson, "Experimental and numerical investigation of an aggressive intermediate turbine duct - Part 2: Flowfield under off-design inlet conditions," in *26th AIAA Applied Aerodynamics Conference, AIAA-2008-7056*, 2008.
- [13] E. Göttlich, F. Malzacher, F. Heitmeir, and A. Marn, "Adaptation of a transonic test turbine facility for experimental investigation of aggressive intermediate turbine duct flows," in *AIAA paper*, 2005. ISABE-2005-1132.

- [14] E. Göttlich, “Research on the aerodynamics of intermediate turbine diffusers,” *Progress in Aerospace Sciences*, vol. 47, no. 4, pp. 249–279, 2011.
- [15] J. Hubinka, C. Santner, B. Paradiso, F. Malzacher, and E. Göttlich, “Design and construction of a two shaft test turbine for investigation of mid turbine frame flows,” in *Proceedings of ISABE*, 2009. ISABE2009-1293.
- [16] R. Spataro, E. Göttlich, D. Lengani, C. Faustmann, and F. Heitmeir, “Development of a turning mid turbine frame with embedded design - part 1: Design and steady measurements,” in *Proceedings of ASME Turbo Expo*, 2013. GT2013-95279.
- [17] R. Spataro, E. Göttlich, D. Lengani, C. Faustmann, and F. Heitmeir, “Development of a turning mid turbine frame with embedded design - part 2: Unsteady measurements,” in *Proceedings of ASME Turbo Expo*, 2013. GT2013-95280.
- [18] N. Billiard, G. Paniagua, and R. Dénos, “Impact of clocking on the aerothermodynamics of a second stator tested in a one and a half stage HP turbine,” *Journal of Thermal Science*, vol. 17, no. 2, pp. 97–110, 2008.
- [19] S. Lavagnoli, T. Yasa, G. Paniagua, L. Castillon, and S. Duni, “Aerodynamic analysis of an innovative low pressure vane placed in an s-shape duct,” *Journal of turbomachinery*, vol. 134, no. 1, pp. 1–13, 2012.
- [20] J. Solano, V. Pinilla, G. Paniagua, S. Lavagnoli, and T. Yasa, “Aero-thermal investigation of a multi-splitter axial turbine,” *International Journal of Heat and Fluid Flow*, vol. 32, no. 5, pp. 1036–1046, 2011.
- [21] C. W. Haldeman, M. G. Dunn, J. W. Barter, B. R. Green, and R. F. Bergholz, “Aerodynamic and heat-flux measurements with predictions on a modern one and one-half state high pressure transonic turbine,” *Journal of turbomachinery*, vol. 127, no. 3, pp. 522–531, 2005.
- [22] C. W. Haldeman, M. G. Dunn, J. W. Barter, B. R. Green, and R. F. Bergholz, “Experimental investigation of vane clocking in a one and 1/2 stage high pressure turbine,” *Journal of turbomachinery*, vol. 127, no. 3, pp. 512–521, 2005.
- [23] I. Qureshi, A. Smith, and T. Povey, “HP vane aerodynamics and heat transfer in the presence of aggressive inlet swirl,” *Journal of Turbomachinery*, vol. 135, no. 2, p. 021040, 2012.
- [24] I. Qureshi, A. Beretta, K. Chana, and T. Povey, “Effect of aggressive inlet swirl on heat transfer and aerodynamics in an unshrouded transonic hp turbine,” in *Proceedings of ASME Turbo Expo*, 2011. GT2011-46038.
- [25] P. F. Beard, A. D. Smith, and T. Povey, “Effect of combustor swirl on transonic high pressure turbine efficiency,” *Journal of Turbomachinery*, vol. 136, no. 1, p. 011002, 2013.

- [26] R. Ainsworth, D. Schultz, M. Davies, C. Forth, and M. Hilditch, "A transient flow facility for the study of the thermofluid-dynamics of a full stage turbine under engine representative conditions," in *ASME, Gas Turbine and Aeroengine Congress and Exposition, Amsterdam, Netherlands*, 1988. 88-GT-144.
- [27] C. Arroyo Osso, L.-U. Axelsson, U. Håll, T. G. Johansson, J. Larsson, and F. Haselbach, "Large-scale low-speed facility for investigating intermediate turbine duct flows," in *AIAA paper*, 2006. AIAA-2006-1312.
- [28] J. Hjärne, J. Larsson, and L. Löfdahl, "Design of a modern test-facility for LPT/OGV flows," in *Proceedings of ASME Turbo Expo*, ASME, 2003. GT2003-38083.
- [29] K. Chana, D. Cardwell, and T. Jones, "A review of the Oxford Turbine Research Facility," in *Proceedings of ASME Turbo Expo*, ASME, 2013. GT2013-95687.
- [30] G. Paniagua, C. Sieverding, and T. Arts, "Review of the Von Karman Institute Compression Tube Facility for turbine research," in *Proceedings of ASME Turbo Expo*, ASME, 2013. GT2013-95984.
- [31] R. J. Anthony and J. P. Clark, "A review of the AFRL Turbine Research Facility," in *Proceedings of ASME Turbo Expo*, ASME, 2013. GT2013-94741.
- [32] M. Dunn and R. Mathison, "History of short-duration measurement programs related to gas turbine heat transfer, aerodynamics, and aeroperformance at Calspan and OSU," in *Proceedings of ASME Turbo Expo*, ASME, 2013. GT2013-94926.
- [33] M. Hilditch, A. Fowler, T. Jones, K. Chana, M. Oldfield, R. Ainsworth, S. Hogg, S. Anderson, and G. Smith, "Installation of a turbine stage in the Pyestock Isentropic Light Piston Facility," in *Proceedings of ASME Turbo Expo*, 1994. 94-GT-277.
- [34] T. Povey, K. Chana, and T. Jones, "Heat transfer measurements on an intermediate-pressure nozzle guide vane tested in a rotating annular turbine facility, and the modifying effects of a non-uniform inlet temperature profile," *Proceedings of the Institution of Mechanical Engineers, Part A: Journal of Power and Energy*, vol. 217, no. 4, pp. 421–431, 2003.
- [35] K. S. Chana, U. K. Singh, and T. Povey, "Turbine heat transfer and aerodynamic measurements and predictions for a 1.5 stage configuration," in *Proceedings of ASME Turbo Expo*, ASME, 2004. GT2004-53951.
- [36] T. Povey, K. S. Chana, T. V. Jones, and M. L. G. Oldfield, "The design and performance of a transonic flow deswirling system - an application of current CFD design techniques tested against model and full-scale experiments," *Advances of CFD in fluid machinery design*, pp. 65–94, 2003.
- [37] M. Goodisman, M. Oldfield, R. Kingcombe, T. Jones, R. Ainsworth, and A. Brooks, "An axial turbobrake," *Journal of turbomachinery*, vol. 114, no. 2, pp. 419–425, 1992.

- [38] P. F. Beard, T. Povey, A. Smith, and P. T. Ireland, “Efficiency of an unshrouded transonic HP turbine: an experimental and computational study,” in *Proceedings of the 8th European Turbomachinery Conference*, 2009.
- [39] I. Qureshi and T. Povey, “A combustor-representative swirl simulator for a transonic turbine research facility,” *Proceedings of the Institution of Mechanical Engineers, Part G: Journal of Aerospace Engineering*, vol. 225, no. 7, pp. 737–748, 2011.
- [40] J. Doorly and M. Oldfield, “The theory of advanced multi-layer thin film heat transfer gauges,” *International journal of heat and mass transfer*, vol. 30, no. 6, pp. 1159–1168, 1987.
- [41] M. Oldfield, “Impulse response processing of transient heat transfer gauge signals,” *Journal of turbomachinery*, vol. 130, no. 2, 2008.
- [42] M. Collins, K. Chana, and T. Povey, “Improved methodologies for time resolved heat transfer measurements, demonstrated on an unshrouded transonic turbine casing,” in *Proceedings of ASME Turbo Expo*, 2015. GT2015-43346.
- [43] T. Povey, M. Oldfield, and F. Haselbach, “Transonic turbine vane tests in a new miniature cascade facility,” *Proceedings of the Institution of Mechanical Engineers, Part A: Journal of Power and Energy*, vol. 222, no. 5, pp. 529–539, 2008.
- [44] A. Main, C. Day, G. Lock, and M. Oldfield, “Calibration of a four-hole pyramid probe and area traverse measurements in a short-duration transonic turbine cascade tunnel,” *Experiments in fluids*, vol. 21, no. 4, pp. 302–311, 1996.
- [45] P. F. Beard, *On Transient Turbine Efficiency Measurements with Engine Representative Inlet Flows*. PhD Thesis, Department of Engineering Science, University of Oxford, 2010.
- [46] M. Johansson, V. Chernoray, L. Ström, J. Larsson, and H. Abrahamsson, “Experimental and numerical investigation of an aerodynamically loaded guide vane in a turbine duct,” in *Proceedings of ASME Turbo Expo*, 2011. GT2011-46221.
- [47] M. Johansson, T. Povey, K. Chana, F. Wallin, and H. Abrahamsson, “Aerodynamic and heat transfer measurements on an intermediate turbine duct vane,” in *Proceedings of ASME Turbo Expo*, 2014. GT2014-26032.
- [48] M. Johansson, H. Abrahamsson, J. Mårtensson, T. Povey, and K. Chana, “Aerothermal measurements and predictions of an intermediate turbine duct turning vane,” in *Proceedings of ASME Turbo Expo*, 2015. GT2015-43449.
- [49] M. Johansson, T. Povey, K. Chana, and H. Abrahamsson, “Effect of low-NOx combustor swirl clocking on ITD vane heat transfer with an upstream HPT stage - an experimental and computational study,” *Submitted to scientific journal*, 2016.
- [50] M. Johansson, T. Povey, K. Chana, and H. Abrahamsson, “Effect of low-NOx combustor swirl clocking on ITD vane aerodynamics with an upstream HPT stage - an experimental and computational study,” *Submitted to scientific journal*, 2016.

A Additional Results

This chapter includes additional results from experiments in the OTRF not published in the appended papers.

Figure A.0.1 show static pressure distributions measured on the ITD endwalls. Tappings were located circumferentially just upstream, in the passage, and just downstream of the ITD vane, covering three passages, as indicated in Figure 4.2.4. The results from tappings upstream of the ITD vane show the presence of the ITD vane with increased static pressure in front of each vane leading edge. There are differences between adjacent passages, as the static pressure of the peaks in front of the ITD vanes and valleys mid-passage vary between passages. The tappings inside the ITD vane passage show the pressure difference from pressure to suction side. Downstream of the ITD vane the static pressure show the presence of the ITD vane wake as peaks in static pressure. Common with the upstream tappings there are differences in peak and minimum static pressure between adjacent ITD passages. Common for all locations is the drop in endwall pressure from the Uniform case to the Swirl 1 case and further to the Swirl 2 case.

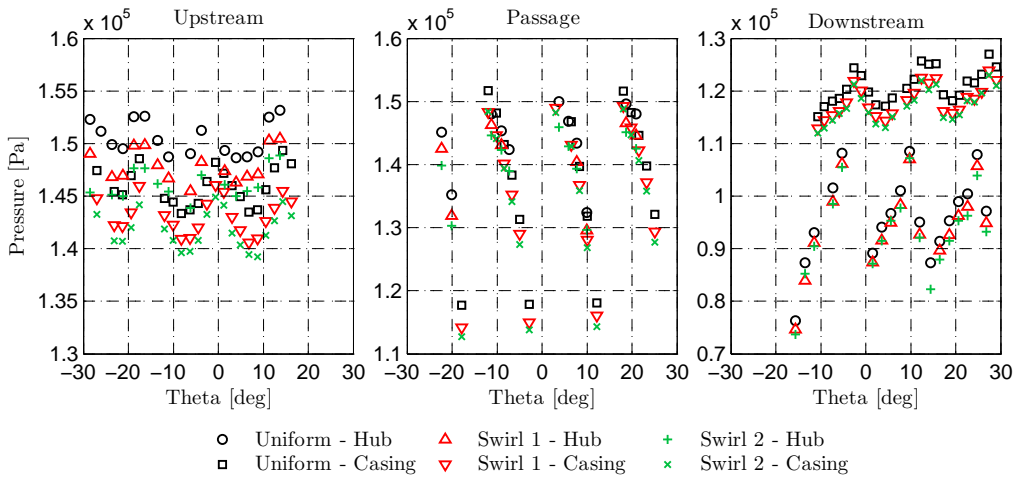


Figure A.0.1: *ITD endwall static pressure*

Static pressure tappings were placed further downstream of ITD vane, both axially along a single circumferential location and circumferentially along a single axial location. The results are presented in Figure A.0.2. As with Figure A.0.1, the static pressure is seen to drop from the Uniform case to the Swirl cases. The circumferential tappings along the hub indicate a large difference between the two adjacent ITD passages covered.

Results from total pressure rakes located approximately 37 mm downstream of the traverse plane with 11 pitot tubes on each rake are included in Figure A.0.3. The rakes are moved around between five different circumferential locations. Common with the total pressure measurements by the traverse probe, there is a total pressure drop from the Uniform case to the Swirl cases. Overall, the shape of the radial profile measured in

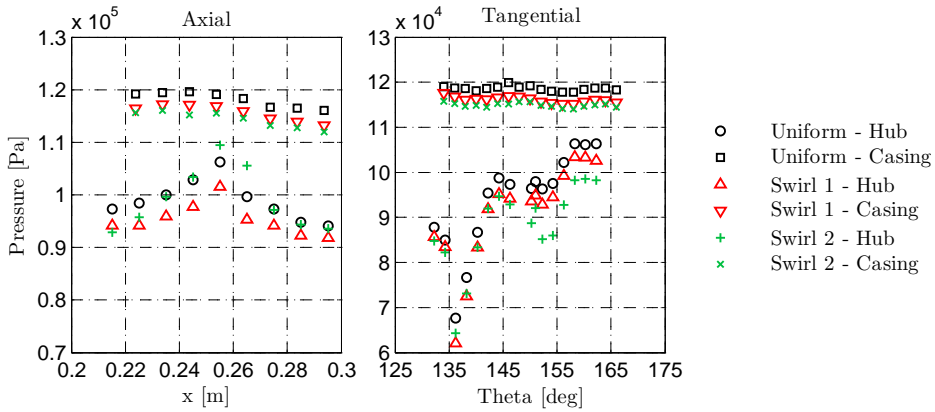


Figure A.0.2: ITD endwall static pressure, axial and circumferential

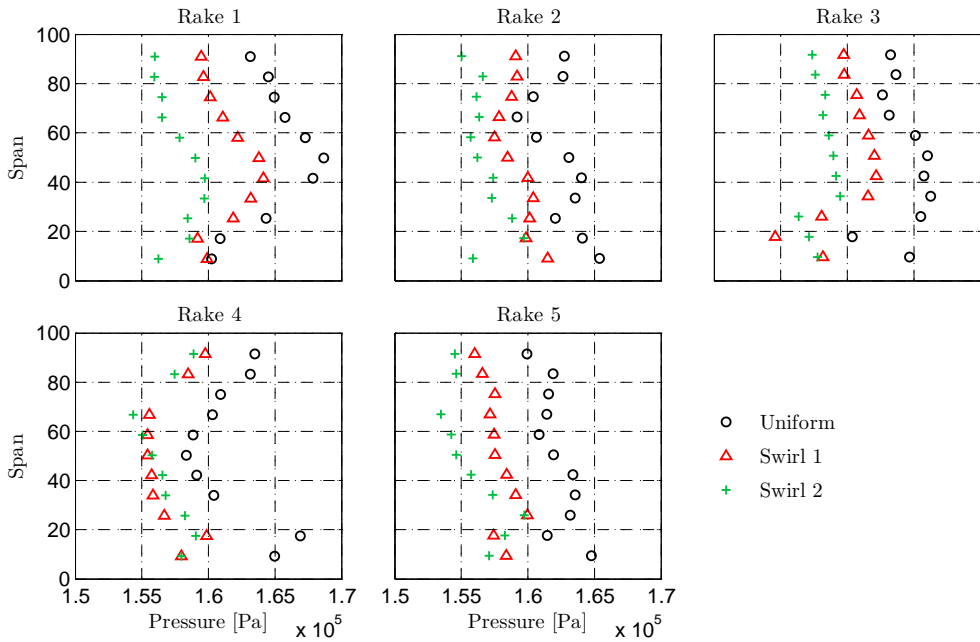


Figure A.0.3: Total pressure measured by radial rakes at five circumferential locations

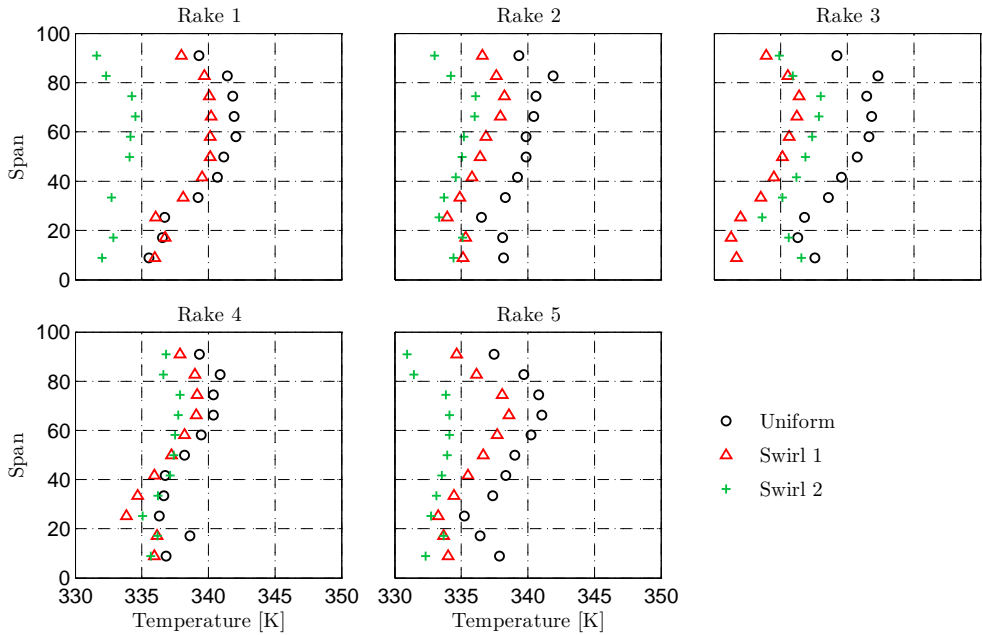


Figure A.0.4: *Total temperature measured by radial rakes at five circumferential locations*

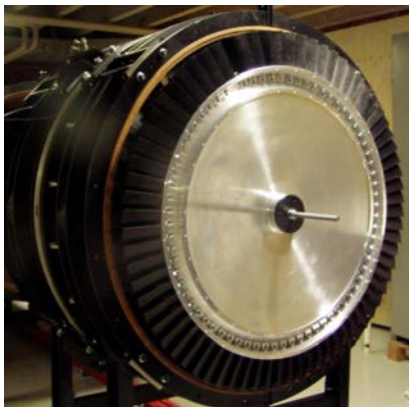
each rake position is not majorly changed with the change in HPT stage inlet condition other than in some local areas.

Total temperature rakes were located approximately 37 mm downstream of the traverse plane with 11 aspirated tubes with a 0.0254 mm K-type thermocouple on each rake. Results from five different circumferential locations are included in Figure A.0.4. A total temperature reduction is noted from the Uniform case to the two Swirl cases. Similar to Figure A.0.3, there are smaller changes in the shape of the radial profile between inlet conditions to the HPT stage.

B Pictures of the experimental facility



Figure B.0.1: Working section of Chalmers LSLS Turbine Facility with traverse system in view



(a)



(b)

Figure B.0.2: (a) HPT rotor in Chalmers Turbine Facility. (b) ITD vane instrumented with static pressure tapings inside the Chalmers Turbine Facility.



Figure B.0.3: *FACTOR ITD vane ahead of instrumentation*

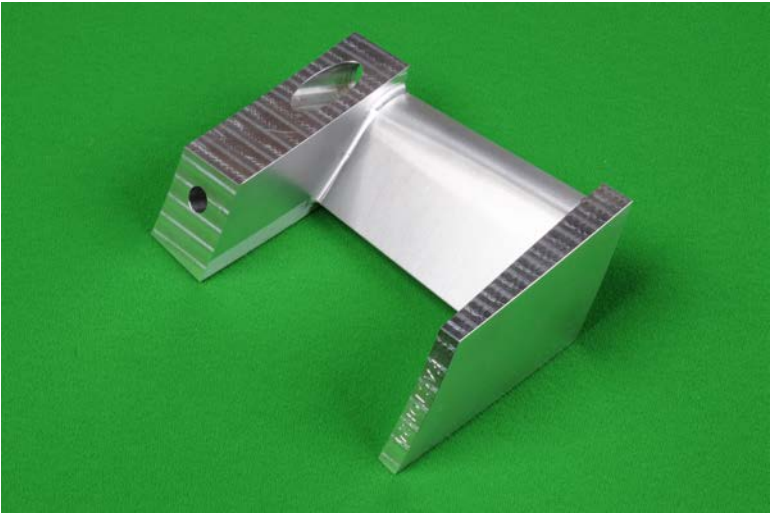
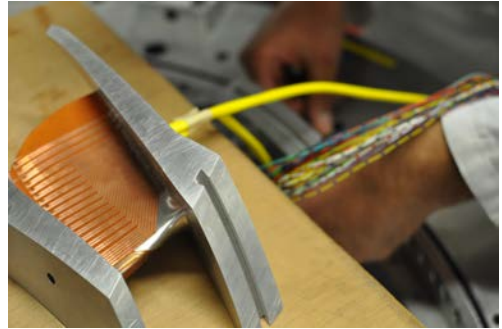


Figure B.0.4: *FACTOR Deswirl vane*



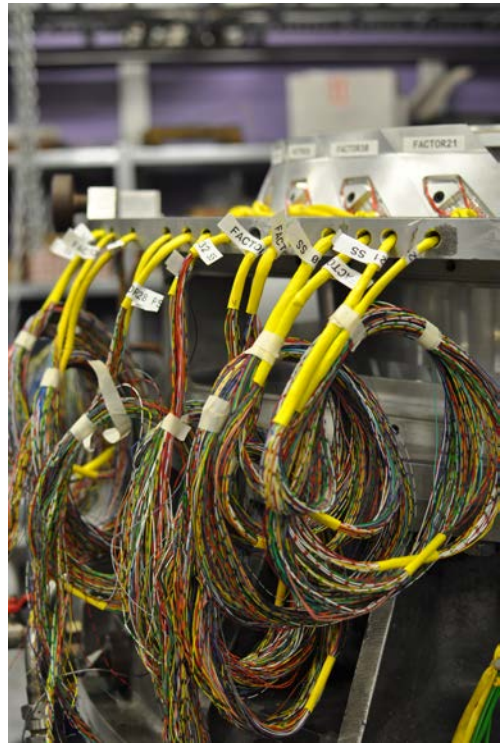
(a)



(b)



(c)



(d)

Figure B.0.5: Assembly of ITD vane ring. (a) holes through centralizing plate through which wires and scanivalve tubes are lead. (b) Feeding wires to TFHFG through centralizing plate. (c) Assembled ITD vanes with TFHFGs, deswirl vanes below. (d) Wires to TFHFGs.

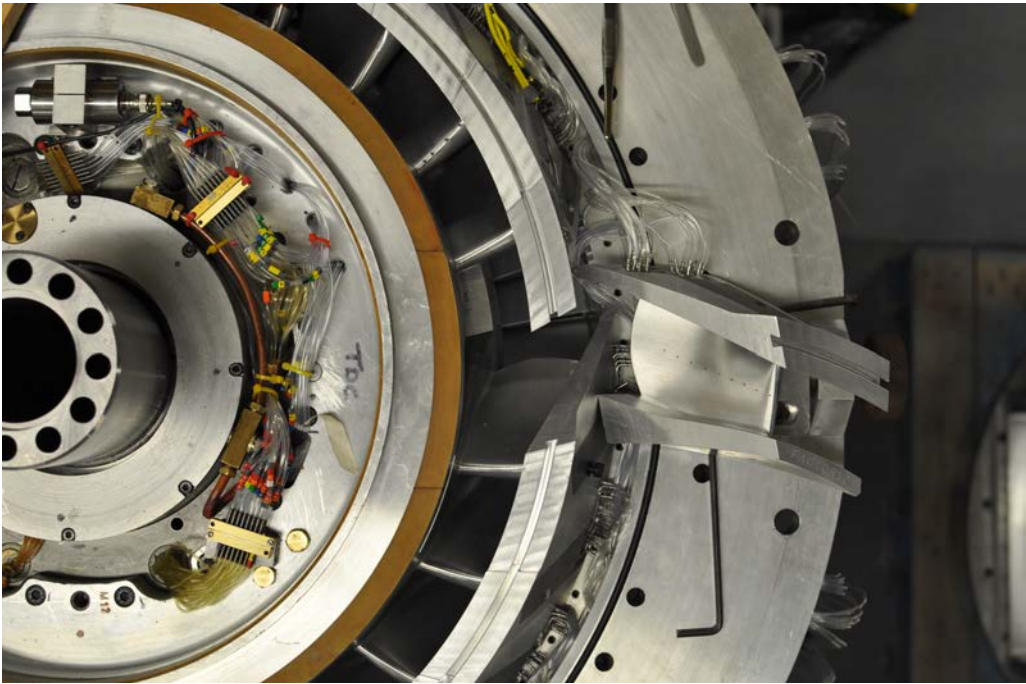


Figure B.0.6: *Assembling the final ITD vane*



(a)



(b)

Figure B.0.7: (a) *MT1 HPT rotor.* (b) *MT1 HPT rotor assembled on top of ITD vane ring.*



Figure B.0.8: *Turbobrake viewed from behind*

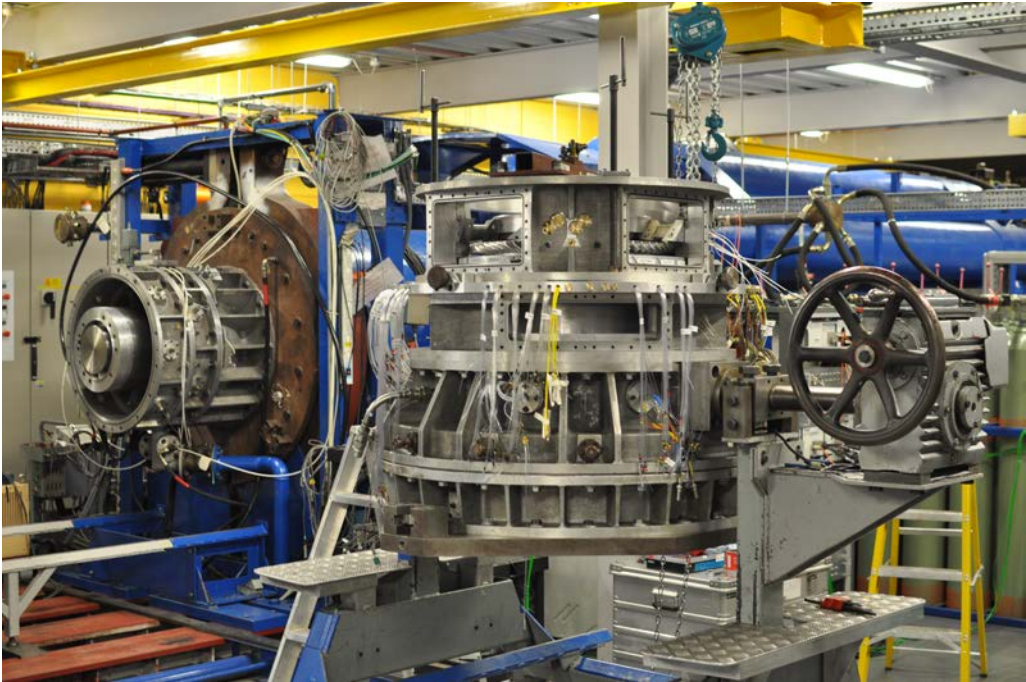
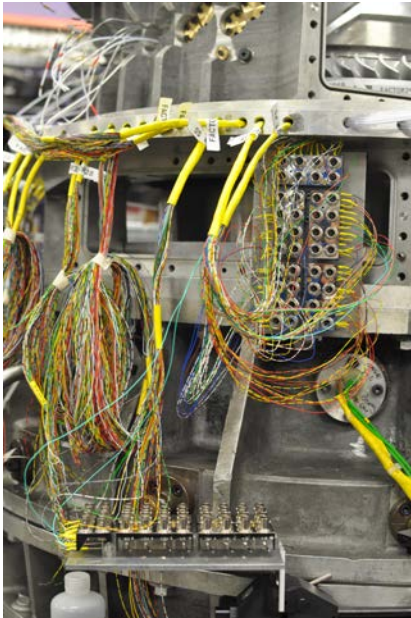
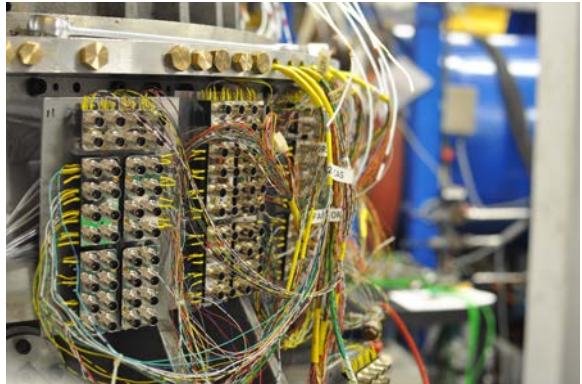


Figure B.0.9: *Partly assembled working section with OTRF in the background*



(a)



(b)

Figure B.0.10: *TFHFG wires soldered onto BNC brackets*

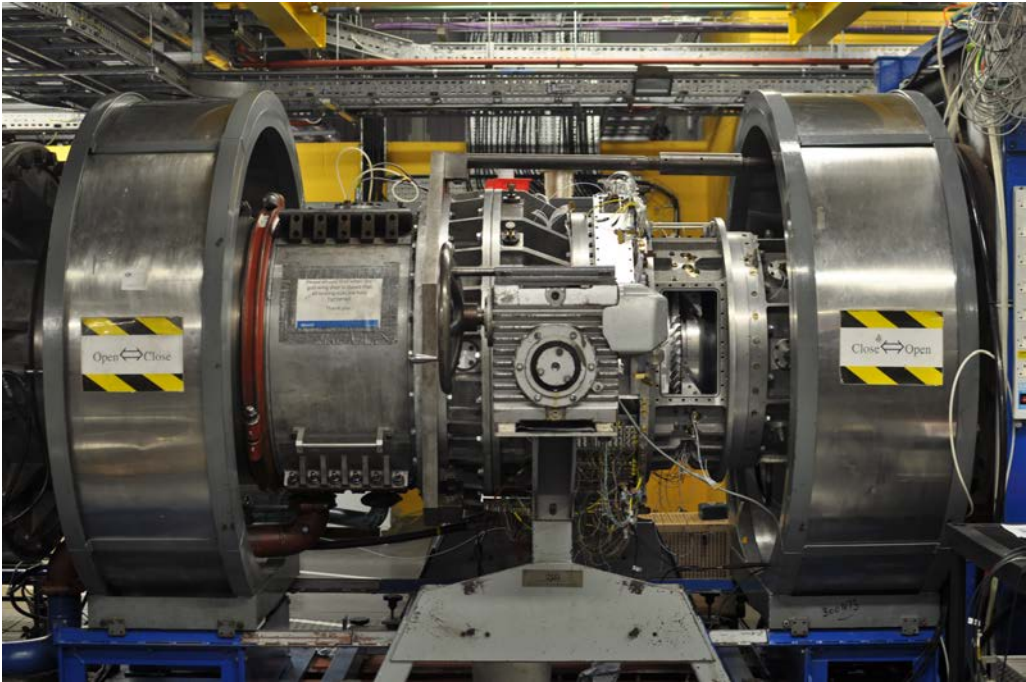


Figure B.0.11: *FACTOR* configuration assembled and installed in the OTRF

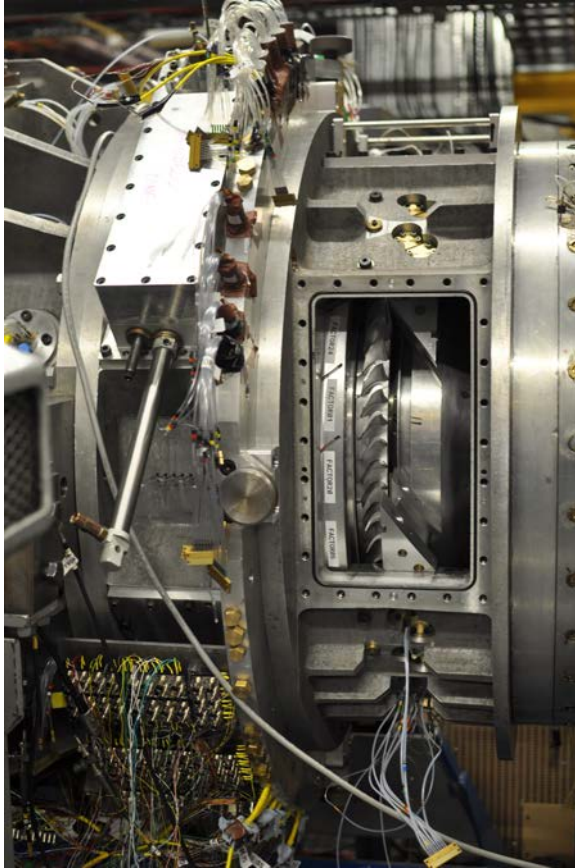


Figure B.0.12: Working section with HPT vane cassette removed allowing HPT rotor and ITD early casing to be seen. ITD exit traverse cassette seen at top left corner.



(a)



(b)

Figure B.0.13: (a) Total pressure rakes mounted in the rake cassette. (b) Total temperature rake.

